Assessing the rockfall protection efficiency of forests at the regional scale

C. Lanfranconi, G. Sala, P. Frattini, G.B. Crosta, A. Valagussa*

Department of Earth and Environmental Sciences, University Milano-Bicocca, Milano, Italy.

*Correspondence to: C. Lanfranconi, Department of Earth and Environmental Sciences, University Milano-Bicocca, Milano, Italy.

E-mail: c.lanfranconi2@campus.unimib.it

Abstract

The aim of this paper is to achieve a quantitative assessment of rockfall protection forest efficiency at regional scale, considering site specific forest, morphological and lithological parameters. At first, a semi-automatic GIS-based method, integrated with a multi-scenario 3D-rockfall model realized by using the simulation code HY-STONE, has been used to map protection forests of Regione Lombardia (central Italian Alps). For each different forest type, a rockfall protective efficiency has been assessed by using empirical (energy line angle) and modelling (HY-STONE) approaches. The empirical approach shows an increase of the energy line angle value from about 36° for the bare slopes to over 40° in forested slopes, with a value ranging from 37° to 44° for different forests types. The modelling approach is based on a new efficiency index EEI ranging from 0 (minimum efficiency, equal to no forest condition) to 1 (maximum efficiency): the efficiency of different forest types ranges from 0.08 to 0.98 by using average values of the controlling parameters. To modulate the efficiency in each single forest at regional scale, a set of parametric simulations was performed to evaluate the effects of controlling parameters. The parametric simulations show that block volume, slope gradient, DBH and forest density are the most important parameters that control the efficiency. These parameters have been used within a multiple linear regression function to associate a protection efficiency to each specific protection forest in the regional map. This allows to discriminate quantitatively the individual forests according to their actual efficiency. Most of the protection forest area (45%) show an efficiency greater than 0.75 and only the 14% of the total covered area show a value lesser than 0.25.

Keywords: protection forest, rockfall, HY-STONE modelling, efficiency, regional scale

Introduction

Forests can play a role at defending structures and infrastructures from rockfalls and avalanches (Jahn 1988; Berger et al. 2002; Dorren et al. 2004a; Perret et al. 2004). Since many decades this role is recognized at regulatory level, as witnessed by the Italian Royal Decree 3267 dating back to 1923, in which it is said that "forests that […] defend lands or buildings from avalanches, the rolling of stones, the fury of the winds […] may, upon request of the provinces, municipalities or other interested institutions and private citizens, be subjected to limitations in their use". Protection forests can be an efficient tool for stopping rockfalls or avalanches detached from upslope or to decrease the probability of primary (for avalanches) and secondary detachments, as in case of unstable blocks located on a debris slope.

The role of forests has been studied in the literature through either empirical (Elkin 2013) and mathematical/numerical modelling approaches (Dorren et al. 2006; Stoffel et al. 2006; Berger and Dorren 2007; Bigot et al. 2009; Jancke et al. 2009; Rammer et al. 2010; Leine et al. 2014; Radtke et al. 2014; Dorren et al. 2015; Kajdiž et al. 2015; Dupire et al. 2016; Moos et al. 2017; Toe et al. 2018). Most of these approaches work at local scale or with synthetic slope to assess the forest efficiency in terms of reduction of the runout (mean or maximum). Only few approaches consider the reduction of kinetic energy (Dupire et al. 2016; Moos et al. 2017) which is fundamental for assessing the effect of forest protection on rockfall hazard. In particular, Dupire et al. (2016) proposed an approach to calculate the efficiency in terms of kinetic energy reduction throughout the forest, as a function of propagation distance. This approach is useful to compare different local-scale forest scenarios into detail but does not provide a single-statistical value to be used for regional scale analysis.

A strong difference exists between local and regional rockfall models. Local rockfall models imply the exact or detailed knowledge of the local conditions, relatively to the topography, exposed lithology, land use and vegetation (Agliardi et al. 2003). All of these are characterized by an important level of stochasticity due to the variability of properties and the difficulty in a full description and use of information (Bourrier et al. 2009; Crosta et al. 2015). At the same time, block characteristics can vary both at the source and during the propagation. At the regional scale the possibility to describe accurately the nature of the slopes and the blocks becomes

extremely difficult because of the inherent variability and the difficulty in accurate data collection over very large areas (Guzzetti et al. 2002; Crosta et al. 2003; Dorren and Seijmonsbergen 2003; Frattini et al. 2008).
In this paper, we present a regional-scale approach to study the effects of forests on rockfalls through surveying, mapping and modelling activities. We propose a semi-automatic GIS-based approach for the identification and characterization of protection forests at regional scale.
The aims of this study are: 1) to identify and map rockfall protection forests at regional scale, 2) to quantitatively assess the efficiency of different forest and land-use types, 3) to study the role of controlling parameters on the efficiency, and 4) to classify the protection forests according to their protective capability.

Study area

The methodology has been applied to the alpine area of Lombardy Region (about 13,740 km^2). This area belongs to the Central Italian Alps (Fig. 1) and ranges in elevation from about 200 m to 4,020 m a.s.l. The geology of the study area encompasses three main structural units: Southern Alps, Pennidic unit, and Austroalpine domain. These units are separated by the regional east-west trending Insubric fault zone. The Southern Alps are characterized by a fold-and-thrust system, with basement and sedimentary cover rocks. The units to the north of the Insubric line consist of the Austroalpine nappes to the east and the Penninic nappes to the west. Austroalpine units consist of metamorphic basement and sedimentary cover detached from their lithosphere during the Cretaceous orogenesis. The Penninic units include remnants of oceanic lithosphere (Malenco-Forno Unit) as well as basement of the European margin (Adula, Tambò and Suretta Units). Two important Tertiary tonalitic to granodioritic intrusions occupy a large part of Valchiavenna (Masino-Bregaglia) and Valcamonica (Adamello). The alpine territory is characterized by high mountains and deep valleys, producing high relief energy. Today, most of the region has a continental climate, characterized by low to medium annual rainfall (between 650 and 2,250 mm/a) mainly concentrated in spring and autumn, cold winters, and high daily and annual temperature fluctuations. Climatic regime at higher elevations is characterized by dry winters and rainy summers.
Geographically, the study area can be roughly subdivided into two subregions: the Lombardy Alps and the Lombardy pre-Alps, located to the north and south of the Insubric line respectively (Marazzi 2005). The Lombardy Alps are characterized by extensive coniferous forests and alpine habitats, with minor deciduous forest at lower elevation. In the pre-Alps, deciduous forests are dominant, with few coniferous forests at higher elevation. The tree line in the alpine area ranges between 1,650 m and 2,450 m a.s.l. (Gehrig-Fasel et al. 2007). In total, the present-day extent of the forest cover amounts to 5,590 km^2, approximately 41% of the study area, whereas in 1954 it covered 4,760 km^2 (35%).

Rockfall inventory

The rockfall inventory has been implemented starting from the landslide database of the Lombardy Region (GeoIFFI, Frattini et al. 2003; Trigila et al. 2010), which reports each landslide as a polygon with alphanumeric attributes. The database was produced and kept updated by the Lombardy Region since 1997. The inventory includes over 1,300 rockfall events for which the date of occurrence is not always available.
Based on bibliographic and archive data sources, the rockfall database has been updated by introducing about 2,000 historical rockfall events ranging from 1950 to 2018 (Fig. 1). The updated database includes the following information (Innocenzi et al. 2017): location, coordinates of the detachment and/or stopping points, date of occurrence, volume, number of casualties, number of injured and/or evacuated, type of structural and infrastructural damage (i.e. functional, structural or aesthetic). For many events, the position was not directly reported in the archive data sources and it was assigned through Google Earth historical imagery or Google Maps Street View. This position is affected by a certain degree of uncertainty that has been qualitatively estimated for each rockfall based on the degree of confidence in the position, ranging from < 10 m to 1 km. The historical inventory forms the basis for a robust calibration of the models and for such a reason these events should be numerous enough to be statistically representative including a certain variability in terms of type of affected trees, forest density and block volumes.

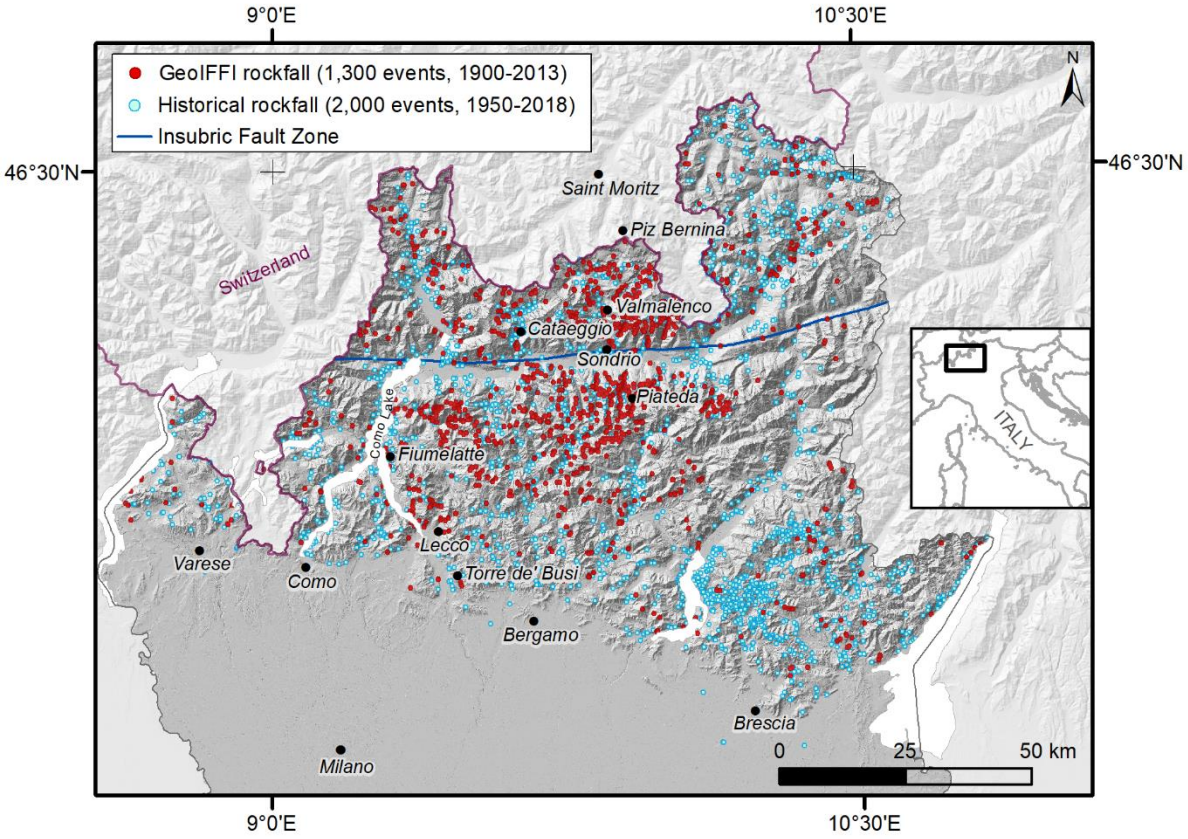

Fig. 1 *GeoIFFI and Historical inventory of rockfalls in Lombardy Region: points represent single events or records.*

Regional forest map

The regional Forest and Land Use (FLU) map was obtained from the regional map of forest types provided by the Regional Forest Agency (ERSAF), integrated with the INFC forest types dataset (INFC 2005, National Inventory of Forests and Carbon Tanks) and with the land cover classes (DUSAF 4.0, Regione Lombardia, 2012) for those areas where the forest information was not available (Fig. 2, Table 1).
For each forest type, the value of DBH (diameter at breast height) and the forest density were provided by ERSAF, based on INFC data (Fig. 3) and on site direct measurements.

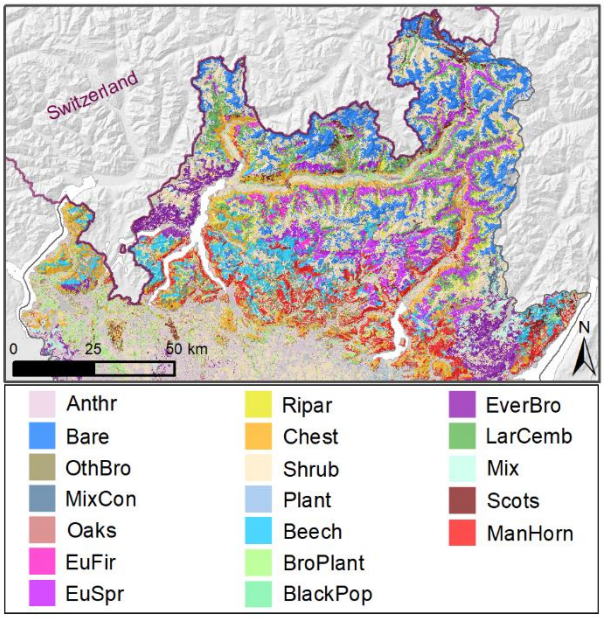

Fig. 2 *Map of the 19 forest types derived from the regional map of forest types by ERSAF and integrated with the INFC (INFC 2005, National Inventory of Forests and Carbon Tanks) and DUSAF (DUSAF 4.0, Regione Lombardia, 2012) datasets.*

Table 1 *Forest and Land-use (FLU) types obtained from forest types provided by ERSAF and integrated with the INFC and DUSAF datasets.*

Forest and land-use types	FLU Symbol	% of study area
Larche and *Pinus cembra* forests	LarCemb	4%
European spruce forests (*Picea abies*)	EuSpr	6%
European silver fir forests (*Abies alba*)	EuFir	<1%
Scots pine forests (*Pinus odelling*)	Scots	1%
Austrian pine (*Pinus nigra*), Larche-Scots pine, Scots pine forests and other pure or mixed coniferous forests	MixCon	<1%
Beech forests (*Fagus*)	Beech	4%
Sessile oak (*Quercus petraea*), pubescent oak (*Quercus pubescens*) and common oak (*Quercus robur*) forests	Oaks	1%
Chestnut forest (*Castanea sativa*)	Chest	5%
Manna ash (*Fraxinus Ornus*) and European hop-hornbeam (*Ostrya carpinifolia*) mixed forests; common hornbeam (*Carpinus betulus*) forests	ManHorn	5%
Riparian forests dominated by grey alder (*Alnus glutinosa*), black alder (*Alnus incana*) and white poplar (*Populus alba*)	Ripar	3%
Other broadleaf forests	OthBro	4%
Evergreen holly oak (*Quercus Ilex*) forests	EverBro	4%
Hybrid black poplar forests (*Populus x canadensis*)	BlackPop	<1%
Other broadleaf plantations	BroPlant	3%
Mixed conifer and broadleaf forests	Mix	1%
Shrub formations	Shrub	26%
Plantations	Plant	1%
Barelands	Bare	8%
Anthropized areas	Anthr	8%

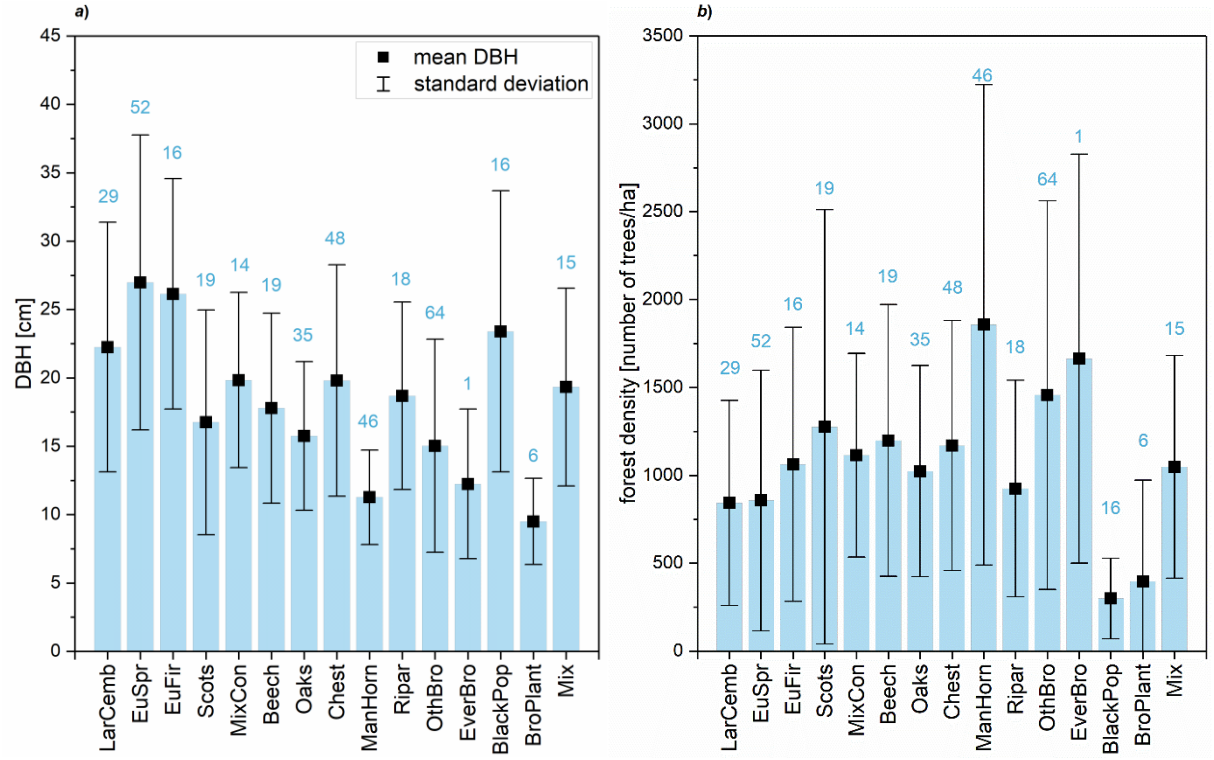

Fig. 3 *a) DBH and b) forest density of each forest type. The number of analyzed forest sample areas, the mean values (black square), and 1 standard deviation (black line) are reported.*

Methods

HY-STONE

HY-STONE (Agliardi and Crosta, 2003; Crosta and Agliardi, 2004; Frattini et al., 2012) is a 3D rockfall simulator based on a hybrid algorithm which is a three-dimensional extension of Pfeiffer and Bowen (1989) and Azzoni et al. (1995). Free fall, impact and rolling are simulated with an empirical approach by using tangential/normal restitution and friction coefficients or with a more advanced elasto-viscoplastic impact model (Di Prisco and Vecchiotti 2006). The stochastic nature of rockfall processes and parameters are accommodated by slope morphology and roughness, and by the random sampling of most parameters from different probability density distributions (e.g. uniform, normal, exponential). Specific model components explicitly account for the interactions between blocks and countermeasures or structures, and fragmentation (Frattini et al. 2012). The protective function of the forest can be considered in two different ways in Hy-STONE (Frattini et al., 2012). In the traditional empirical approach, the values of parameters controlling energy dissipation are modified to account for the forest, e.g. increasing rolling friction and reducing the tangential restitution coefficient. As an alternative, a physically-based approach can be adopted by including the effects of trees on rockfall dynamics with a stochastic approach for tree impact (Dorren et al., 2006). This second option requires two raster files defining the tree density and the forest type, and an additional text file containing, for each pixel, detailed forest information such as (i) tree type (ii) heights of stem [m], (iii) average heights of tree [m], (iv) average DBH [m], (v) size of crown of tree [m], (vi) minimum distance between impacts [m], (vii) and maximum amount of kinetic energy that could be dissipated by a tree [J]. Output results include rockfall frequency, trajectory height, rotational and translational velocity, and kinetic energy. At each computed point along fall paths, information is given on type of motion, the energy and 3D position. For tree-impact algorithm the simulator provides the location of impacts, the absorbed energy, and the deviation angle.
The HY-STONE simulator has been used for three different aims: 1) the identification of sectors of slope laying above the elements at risk potentially impacted by rockfalls, 2) the simulation of rockfall scenarios; 3) the parametric simulation of parameters controlling the efficiency. The first two aims listed above have been performed to identify and map the protection forests at the regional scale, while the latter to quantify their protection efficiency.

Protection forest mapping

Identification of sectors of slope laying above the elements at risk

The first requirement for the identification of the protection forests is that, by definition, they need to lay upslope of the elements at risk to be protected. In order to identify and map slope sectors above the elements at risk, a first HY-STONE high-mobility scenario (SC_HMOB) has been performed to trace trajectories that intersect the potential structures and infrastructures. This scenario is not intended to be realistic but aims at simulating the maximum potential runout in order to reach the most distal elements at risk. For this, a 20 m grid size DEM was preferred in order to smooth the topography and increase the runout distance. Moreover, the runout was boosted by using a single parameterization with a low rolling friction coefficient (0.4) and high normal and tangential restitution coefficients (65). The source areas of trajectories have been derived from a regional map created through photointerpretation of 1:30.000 colour stereo-photographs (Frattini et al. 2003), integrated with steep areas having a slope-gradient higher than 40° (obtained from the 5 m Lombardy DEM). For each source cell, 5 spherical blocks with a volume of 0.52 m^3 and a density of 2700 kg/m^3 has been simulated.

Calibration of the model and simulation of most-likely rockfall scenario

The second requirement for the identification of the protection forests is that they need to be located in areas potentially impacted by rockfall. With respect to the previous scenario, we needed to perform a new regional scale rockfall model that use realistic rolling friction and tangential and normal restitution coefficients, in order to simulate the most-likely runout. This requires defining the spatial distribution of the coefficients of restitution and rolling friction that control the behaviour of block moving along the slope, and to calibrate the values of such parameters. The first was obtained by creating a unique-condition map of land-use and lithological units, to which we can assign different value of the parameters. The calibration was then accomplished by back-simulating 30 actual rockfall events (SC_CAL) within different lithological and morphological settings. This most-likely scenario has been simulated by using parameters that do not take into account the presence of forest by setting the restitution and friction coefficients of equivalent bareland in forested areas. This allowed us to identify the extent that rockfall would reach in case of forest removal (e.g. wildfires, land-use change). The rockfall source area of most-likely rockfall scenario is the same used for SC_HMOB model. In total, 260,000,000 spherical blocks of 0.52 m^3 have been simulated (10 spherical blocks with a radius equal to 0.5 m and a density of 2700 kg/m^3 from each source cell).

Semi-automatic protection forest mapping

By using the rockfall models, a semi-automatic GIS-base methodology was applied to identify and map the rockfall protection forests, by six main steps (Fig. 4):
1) selection of rockfall trajectories of the high-mobility scenario (SC_HMOB) that intersect the elements at risk (railways, roads and building);
2) 10-m buffering of the selected trajectories;
3) correction of polygons to remove holes within rockfall zones;
4) selection of polygons laying upslope of the elements at risk by comparing the mean elevation of areas affected by rockfalls with the median element-at-risk elevation. This allows to obtain the slope sectors above the elements at risk;
5) intersection of these slope sectors with the polygons obtained by applying steps 2) and 3) to the trajectories of the most likely runout scenario (SC_EXPECTED). This results in the Rockfall Protection Zones (RPZone).
6) Intersection of RPZone with the regional Forest and Land Use (FLU) map to obtain the rockfall protection forests.
A post-processing visual check was required, in particular to reshape protection areas crossed multiple times by hairpin roads. In these cases, the comparison between elevations would have identified only the area located above the highest hairpin turn.

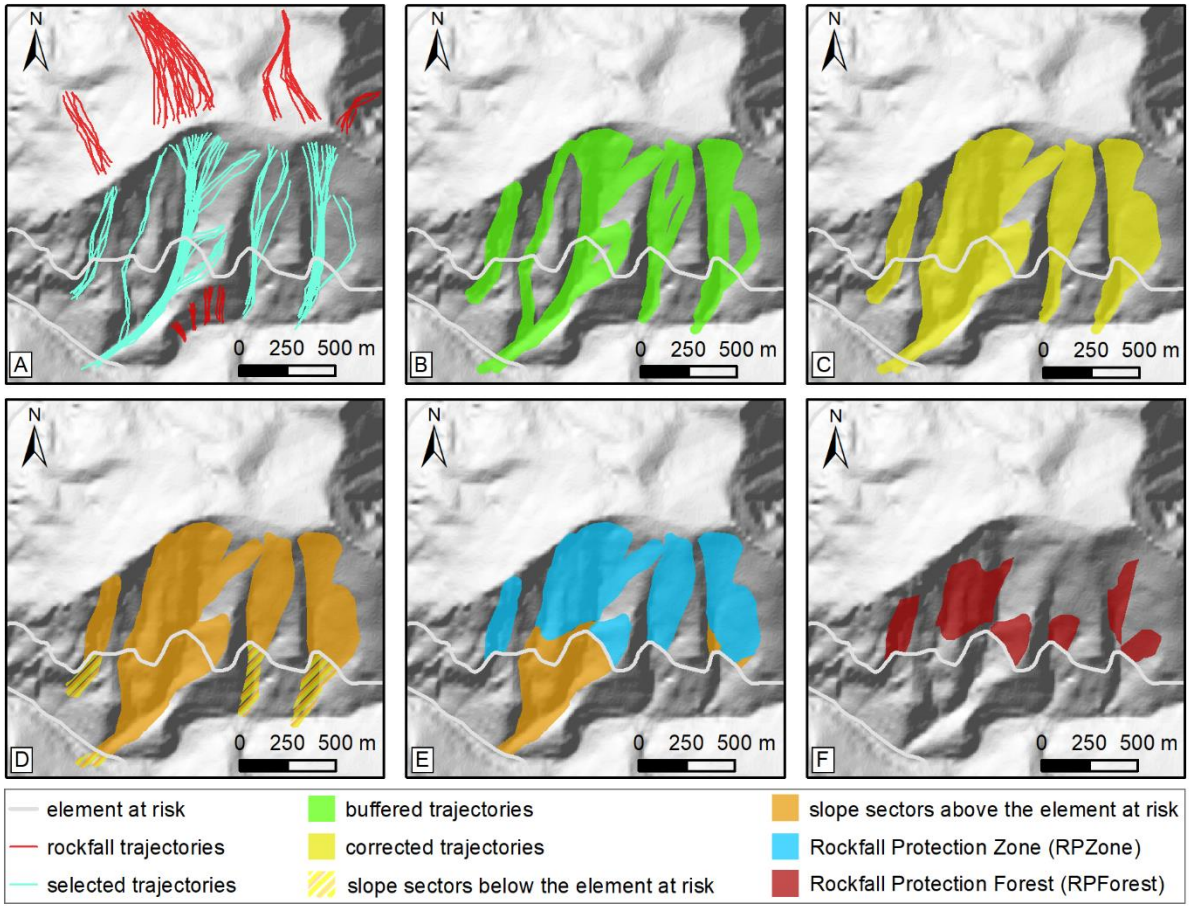

Fig. 4 *Steps of the semi-automatic method for the mapping of the protection forest: a) selection of the trajectories that intersect the element at risk; b) buffering of the selected trajectories; c) polygons correction; d) discrimination of the polygon by position occupied with respect to the element at risk; e) intersection of the sectors that lay above the elements at riskwith the polygons obtained by the SC_EXPECTED to obtain the RPZone and f) intersection with the FLU (forest and land use map).*

Forest efficiency

The protection forest efficiency was assessed through empirical and physically-based approaches, by analyzing the energy line angle and by running HY-STONE models with the forest algorithm.

Energy line

In order to calculate the energy line angle, the difference in elevation (H) and the planar distance (L) of the highest (in the rockfall source area) and the lowest (in the deposit area) points of each rockfall polygon has been extracted. The energy line angle corresponds to $\tan^{-1}(H/L)$, which describes the inverse of the mobility efficiency of the rockfall: the higher the H/L (and the angle), the lower the rockfall mobility. The energy line angle increase in presence of forest has been analysed by Meissl (1998) and Dorren et al. (2005); in this study it has been analysed both for rockfalls that took place entirely within a single forest type (*single forest*), and for those crossing different forest types, computing for each rockfall polygon the prevalent forest type (*prevalent forest*).

Energy Efficiency Index

For characterizing forest efficiency, a new “Energy Efficiency Index (EEI)” is proposed:

$$EEI = 1 - \frac{AUC_{forest}}{AUC_{no\ forest}} \quad [1]$$

where AUC_{forest} and $AUC_{no\ forest}$ are the Area Under Curve of the total kinetic energy of falling blocks as a function of the distance from the source area for both the scenario with forest and the corresponding scenario without forest, respectively (Fig. 5) (see Supplementary Table 1). The EEI ranging from 0 (no efficiency) to 1 (full efficiency). Full efficiency occurs when blocks completely loose the energy as soon as they enter the forest.

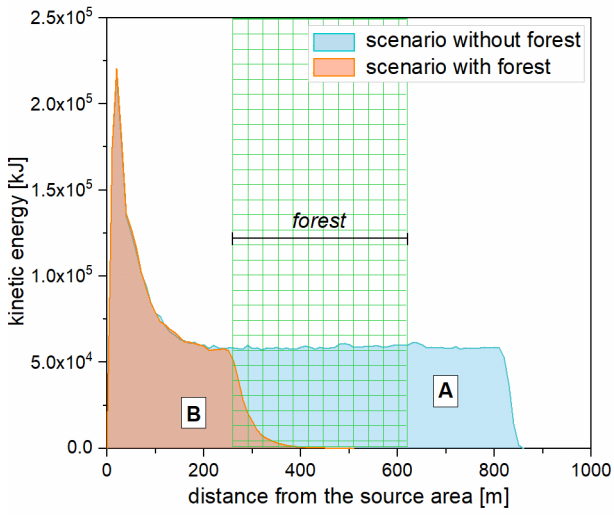

Fig. 5 *The lines represent the total kinetic energy of rockfalls, for slopes without forest (A) and with forest (B). The two areas under the curve (AUC) are used to compute the forest efficiency index (EEI).*

Efficiency of forest types

To calculate the efficiency of different protection forest types with a modelling approach, a set of 30 HY-STONE simulations (SC_FOR) has been performed by using the tree-impact algorithm along a 1000 m-long synthetic DEM with a resolution of 2 m. The synthetic slope has three different sectors: a 40 m-long steep sector with an inclination of 60°, a 800 m-long sector with an inclination of 30°, and a bottom flat sector with an inclination of 5°. The rockfall source area is located on the top of the steep sector. For each FLU forest type, mean values of DBH and of forest density have been used. Starting from these values, the trunk height, the tree height, the crown extent and the maximum absorbable energy have been calculated by using empirical equations (La Marca, 1999; Hemery et al., 2005; Dorren and Berger, 2006). The simulations were performed with a forest length of 350 m, distance of the forest from the source area of 250 m, rolling friction coefficient of 0.5, normal and tangential restitution coefficients of 0.7. Two sets of simulations have been performed by launching 750 spherical blocks of 0.52 m^3 and 1 m^3, respectively, with a density of 2700 kg/m^3.

Sensitivity of protection efficiency

The analysis of the role of controlling parameters on the protection efficiency is necessary to understand how efficiency can vary in different forest, morphological and lithological conditions and for assigning a single efficiency value to each protection forest.
A set of 48 simulations (SC_SENS) were run for the sensitivity analysis by simulating 750 spherical blocks (density 2700 kg/m^3) along the same synthetic slope and DEM used above. Only one forest type with medium efficiency (ManHorn) was used for these models by varying one at a time the following parameters: slope gradient (23°, 25°, 30°, 35°, 37°, 40°, 41°, 43°, 45°), length of the forest (75 m, 100 m, 200 m, 225 m, 300 m, 375 m, 450 m, 525 m), position of the forest (68 m, 200 m, 342 m, 410 and 478 m from the cliff base), DBH and tree density (mean value of each forest type, obtained from a statistical analysis of data provided by ERSAF, varied with a factor of 0.25, 0.5, 0.75, 1.25, 1.5, 1.75 and 2), block radius (0.25 m, 0.35 m, 0.5 m, 0.75 m, 1 m, 1.25 m, 1.5 m, 2 m) (see Supplementary Table 1).

Efficiency classification of protection forests

A multivariate statistical analysis has been performed to calculate the protection efficiency of each polygon of protection forest in Lombardy Region. A multiple linear regression model in the form:

$$EEI = a + b_1x_1 + b_2x_2 + \cdots + b_nx_n \quad [2]$$

where a is a constant, x_i are the n variables and b_i are the regression coefficients, is obtained. The dataset used for the regression is composed of the 30 simulations SC_FOR, the 48 simulations SC_SENS, and further 103 simulations (SC_REG) obtained by randomly varying the values of the parameters along the synthetic slope described above. The multiple linear regression was performed by using IBM SPSS Statistics software (IBM Corp. Released 2017. IBM SPSS Statistics for Windows, Version 25.0. Armonk, NY: IBM Corp.).

Analysis and results

Protection forest mapping

The slope sectors that lay above the elements at risk, as calculated from the high-mobility scenario (SC_HMOB), cover a total area of 1230 km^2 (orange polygons in Fig. 8). In order to map the Rockfall Protection Zones within these sectors, we needed to calibrate the coefficients of tangential and normal restitution and rolling friction (Table 2) by back analysis of thirty real rockfall events (SC_CAL models). In the back analysis, the parameters were calibrated through trial and error approach by fitting the total length of the rockfall events. This length was defined through field mapping of the arrest point positions for 7 case studies; for the others, the rockfall-inventory polygon extent has been used. Four examples of back-calibration are illustrated in Fig. 6, together with a further case study used for validation (Fig. 7). From a visual inspection, the trajectories simulated with the calibrated models appear to reasonably fit the actual rockfall extent in terms of runout distance (Fig. 6), while the lateral dispersion appears to be underestimated, probably due to the low resolution (5 m cell size) of the DEM.

Table 2 *Calibrated values of tangential and normal restitution and rolling friction coefficients obtained from the back analysis of thirty real rockfall events.*

	built area			**sparse built area**			**roads**			**bareland**		
	EN	*ET*	*AT*	*EN*	*ET*	*AT*	*EN*	*ET*	*AT*	*EN*	*ET*	*AT*
alluvial deposits	0.25	0.30	0.82	0.33	0.35	0.73	0.45	0.60	0.30	0.42	0.58	0.53
alluvial fan deposits	0.24	0.30	0.82	0.33	0.36	0.75	0.45	0.60	0.30	0.45	0.62	0.47
debris deposits	0.26	0.28	0.84	0.32	0.40	0.76	0.45	0.60	0.30	0.44	0.53	0.56
talus deposits	0.31	0.37	0.79	0.33	0.37	0.79	0.40	0.52	0.48	0.46	0.55	0.64
glacial deposits	0.26	0.28	0.84	0.32	0.40	0.76	0.45	0.60	0.30	0.44	0.53	0.50
outcrop - limestones, dolostones and marbles	0.20	0.28	0.80	0.31	0.37	0.74	0.45	0.60	0.30	0.65	0.78	0.42
outcrop - granitoid rocks	0.30	0.32	0.85	0.34	0.38	0.82	0.45	0.60	0.30	0.70	0.80	0.43
outcrop - orthogneiss	0.30	0.32	0.85	0.34	0.40	0.79	0.45	0.60	0.30	0.60	0.70	0.43
outcrop - paragneiss, phyllite and serpentinite	0.20	0.28	0.80	0.31	0.37	0.74	0.45	0.60	0.30	0.60	0.72	0.45
outcrop - layered argillites, marl and limestones	0.25	0.29	0.86	0.28	0.38	0.78	0.45	0.60	0.30	0.50	0.62	0.45
outcrop - conglomerates, sandstones	0.24	0.30	0.88	0.32	0.35	0.81	0.45	0.60	0.30	0.59	0.70	0.46

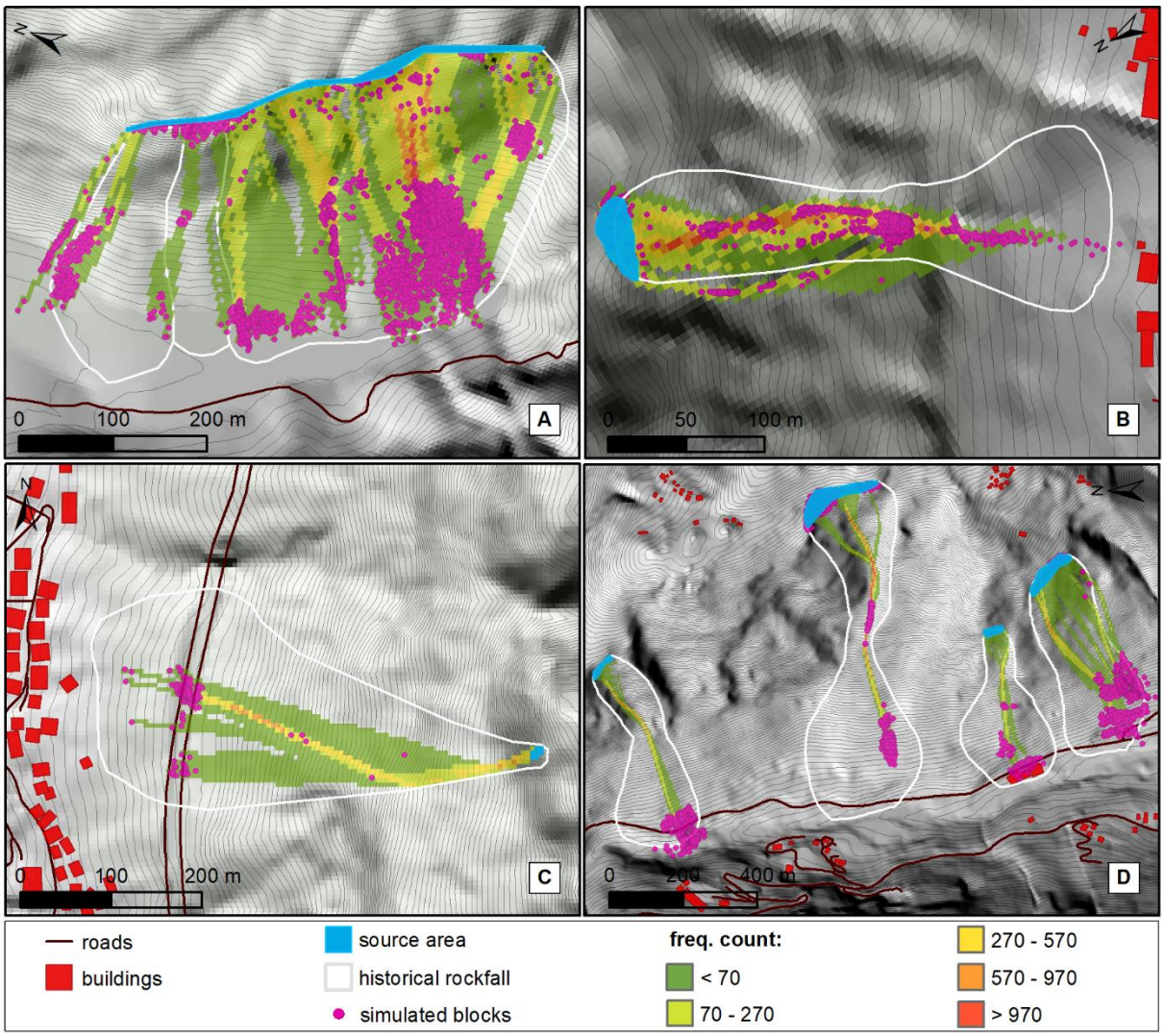

Fig. 6 *Model calibration results: comparison between the mapped historical rockfalls (white polygons) and the simulation results (colours) in 4 of the 31 case studies used to calibrate the regional scale model: a) Piateda (SO) 1960s event, b) Torre de' Busi (LC) 1991 event, c) Fiumelatte (LC) 2010 event, d) Valmalenco (SO) 1987 event. The historical rockfalls of the landslide database of the Lombardy Region (GeoIFFI, Frattini et al. 2003; Trigila et al. 2010) have been mapped through photointerpretation at the regional scale, resulting in polygons slightly larger than the simulated rockfalls. See Fig. 1 for the location of the case studies. The calibrated models fit well the total length of the rockfall event, with some problems in reproducing the lateral extent. This problem is due to the relatively low resolution (5x5 m) and the small roughness of the DEM, as already observed in the literature (Crosta and Agliardi 2004; Frattini et al. 2013), which cause topographic channelling.*

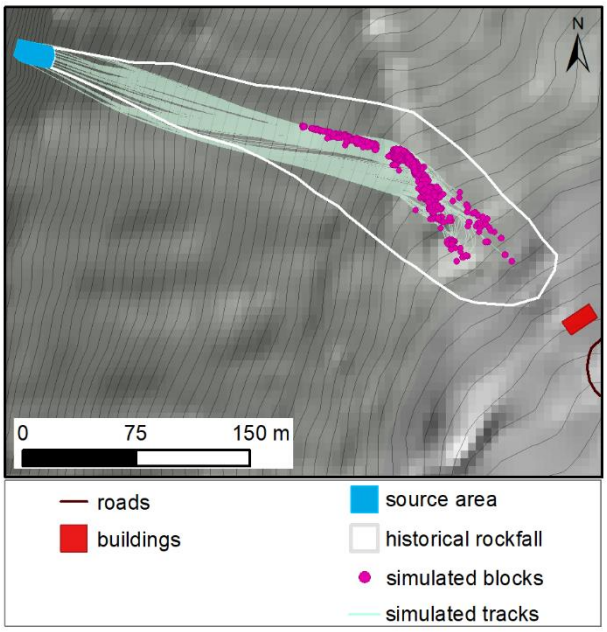

Fig. 7 *Comparison between the Cataeggio 2019 rockfall (withe polygons) and the simulation performed by adopting the parameter values calibrated on the set of case studies (see Fig. 1 for the location of the event). This additional simulation was performed to validate the regional scale calibrated parameters, well fitting both the longitudinal extent and the lateral dispersion of the event, and providing confidence on the reliability of the calibration.*

By using the average values of the calibrated coefficients, we could run a regional-scale rockfall scenario, from which we obtained a total area of 458 km^2 of Rockfall Protection Zones (RPZone) (light blue polygons in Fig. 8). The total area occupied by the RPZone amounts to about 37% of the sectors above the elements at risk (Fig. 8).

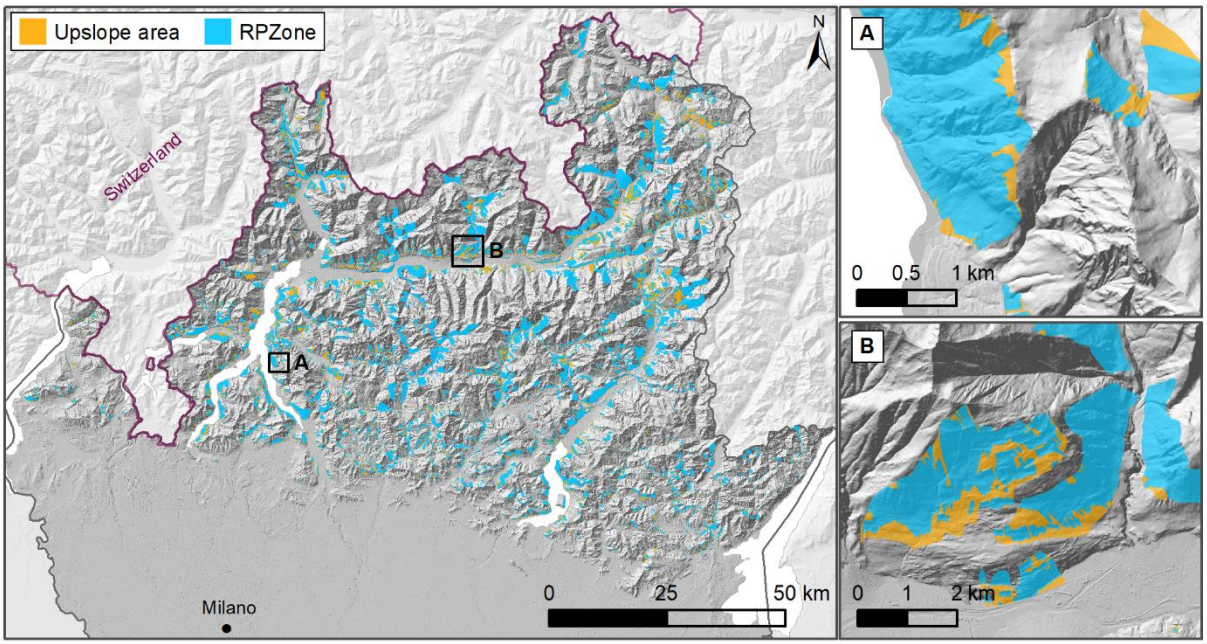

Fig. 8 *Map of the potential rockfall runout: in orange the slope sectors laying above the elements at risk, in light blue the Rockfall Protection Zone (RPZone).*

Regional map of protection forest

The intersection of the RPZone with the regional Forest and Land Use (FLU) map allows to obtain the Rockfall Protection Forests (RPForest) of the entire Lombardy Region (Fig. 9). The presence of some fragmented areas and holes in the map is related to the intersection with FLU map: no forested areas result in lacking information. Through this map, it becomes feasible to identify rockfall protection forests and the protected infrastructures over the entire Lombardy Region:

- the forested area occupies 42% of the total Alpine area of Lombardy Region, and 16% of this is occupied by protection forests (the extent of the rockfall protection forests is about 7735 km^2);
- around 3,500 km of roads out of 30,000 km (12%) and around 37 km of railways out of 900 km (4%) could be potentially protected by forests in case of rockfall events.

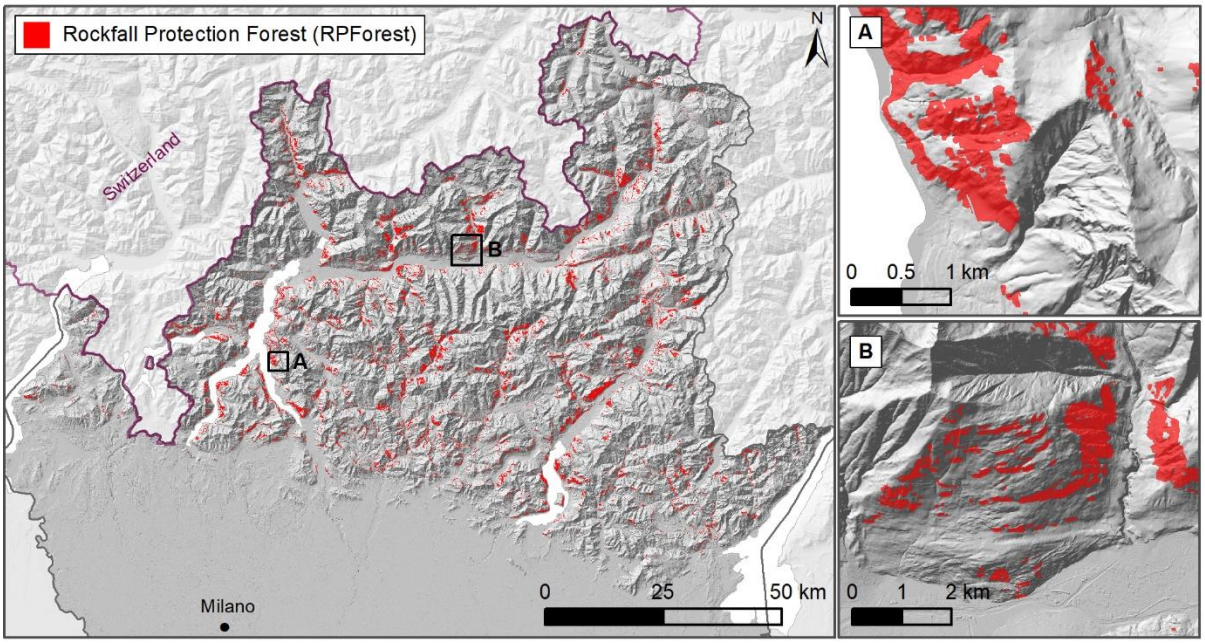

Fig. 9 *Map of the rockfall protection forests (RPForest) in the Alpine area of Lombardy region. RPForest covers 16% of the forested areas.*

Forest efficiency

The energy-line angle calculated considering the prevalent forest type in the areas affected by the rockfall events shows average values ranging from about 36° (Shrub, Bare) up to almost 45° (Oaks). Most of the other forest types show an energy line between 28° and 40°, Considering that the lower the angle, the higher is the rockfall runout, it is possible to see that the presence of forest reduces the energy line angle of about 3-5 degrees, passing from 36° in non-forested areas (e.g., Barelands) to over 40° in forested types. In general, a clear difference between broad-leaved forests and conifer forests is not visible (Fig. 10).
Comparable results were obtained by considering only rockfalls falling completely within a single FLU, to avoid disturbing effects due to the co-presence of different forest types (see Supplementary Figure 1).

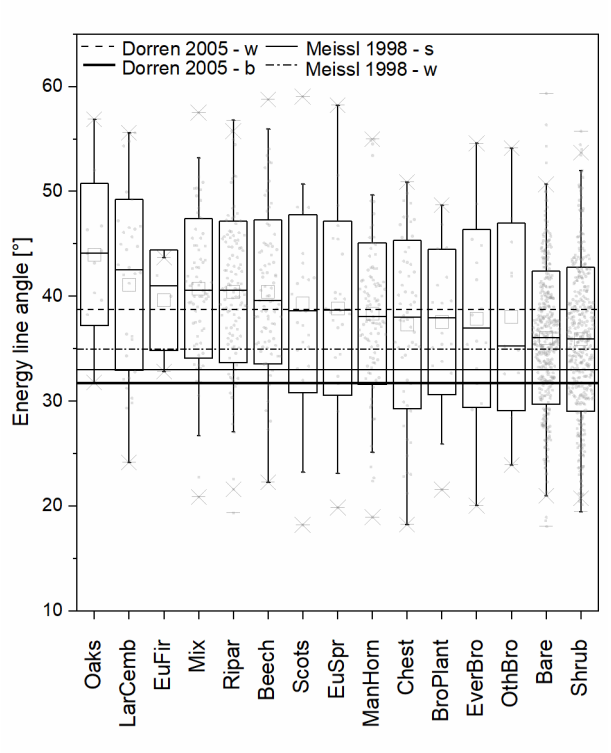

Fig. 10 *Energy line angle distributions for the prevalent forest type within the rockfall polygons. The different lines represent energy line reported in literature. The different lines represent energy line reported in literature. For forested area Meissl (1998) proposed an energy line value of 35° (dash dot line -w), while Dorren et al. (2005) suggested a value of 38° (dashed line - w). For bare and shrub areas, a 32° and 33° value respectively have been proposed by Dorren et al. (2005)(thick continuous line, -b) and Meissl (1998) (continuous line, -s).*

The analysis of forest efficiency with the modelling approach (SC_FOR) has been performed with two classes of block volume. With a block volume of 0.52 m^3, most of the forest types have an EEI of about 0.95 (Fig. 11), except for the ManHorn (EEI = 0.57) and BroPlant (EEI = 0.09) forest types. The resulting efficiencies are squeezed within a narrow range around the maximum values due to the limited size of the blocks. With a block volume of 1 m^3 the values of forest efficiency show a greater dispersion: many types lay between 0.2 and 0.8, the ManHorn type takes an EEI value of 0.23, while the BroPlant type passes to 0.05.

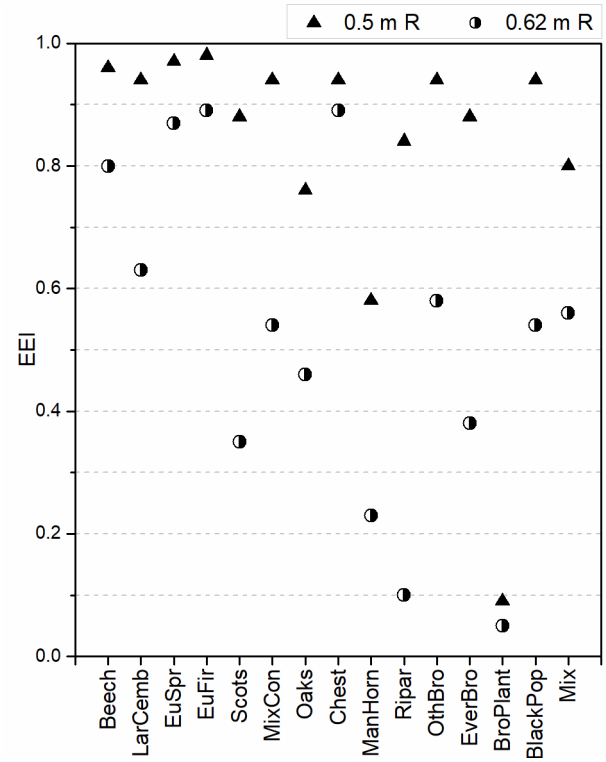

Fig. 11 *Forest efficiency values (triangles) obtained modelling each forest type under the same standard morphological constrains (0.5 m block radius, corresponding to 0.52 m^3), most of the EEI values lays within a narrow range close to the upper bound; BroPlant, ManHorn and EuFir got the minimum intermediate and maximum values, respectively. Forest efficiency values (disks) obtained modelling each forest type and a 0.62 m block radius (1 m^3).*

The sensitivity analysis (SC_SENS) performed on the ManHorn forest type shows that the most affecting parameters are: block volume, slope gradient, DBH and forest length. For these parameters the sensitivity curves show the largest changes (i.e. they are steeper). Forest position is less important. Forest density shows a minor influence for values lower than the mean value (Fig. 12). The EEI is inversely related to the slope gradient and the block radius, and directly proportional to the parameters related to the forest maturity and density (Fig. 12).

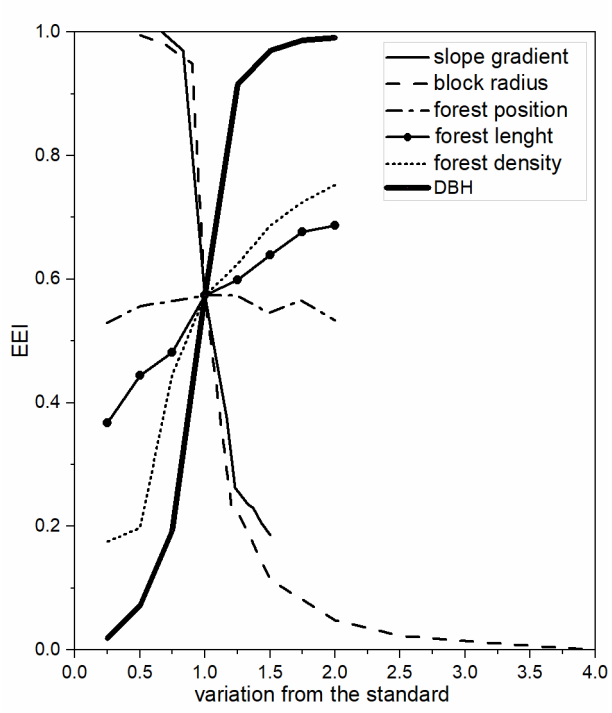

Fig. 12 *Results of the EEI sensitivity analysis: block volume, slope gradient, DBH and forest density are the most influential parameters in defining forest efficiency.*

By using the results of the 180 parametric HY-STONE simulations (SC_FOR + SC_SENS + SC_REG), the following linear multiple regression was obtained:

$$EEI_i = 4.321 - 1.906 * \mathrm{Log}(slope) + 1.211 * \mathrm{Log}(DBH) + 1.250 * density_{forest} + 2.828^{-5} * position_{forest} - 0.668 * radius_{block} + 0.001 * length_{\ forest} \quad (2)$$

Forest type is missing here because already included in the DBH and density values which are specific for each forest type.

Table 3 *SPSS coefficients for the multi regression model.*

Model	Coefficients[a,b]		
	Unstandardized		**Standardized**
	B	Std. Error	Beta
(constant)	4.321	.386	
Log(slope)	-1.906	.267	-.393
Log(DBH)	1.211	.093	.633
forest density	1.250	.320	.191
forest position	2.828E-5	.000	.007
block radius	-.668	.075	-.444
forest length	.001	.000	.262

The analysis has been performed and calibrated on 70% of the 180 parametric models, then validated on the remaining 30%. All requested variables entered the model, obtaining an error R Square greater than 0.65 in both calibrated and validated models: $R^2_{70\%}$=0.77 and $R^2_{30\%}$=0.67. Signs of the coefficients in Table 3 indicate the relation of proportionality between parameters and efficiency (directly proportional when positive and inversely when negative). Standardized coefficients express the importance of each variable in the regression, supporting what observed in the sensitivity analysis, i.e., block radius and DBH are the most important sensitive parameters.
The resulting function can be used to assign an EEI value to each forest polygon, for which the following parameters was calculated:

- average *DBH* and *forest density* of each forest types;
- *Slope gradient, Forest length, position* and *Block radius.*

The *Block radius* has been associated to each polygon based on the lithology of the rockfall source area (or the prevalent lithology where there is more than one lithology in the same source area). To assign a volume to each lithology, the lithology of the source areas has been reclassified into 13 classes, starting from the 1:250,000 scale geological map of Lombardy Region (Fig. 13). Successively, the grain size distribution of at least 9 representative talus deposits for each lithological class has been analysed by using a Wolman's sampling method (Wolman, 1954). This is a standard method in fluvial sedimentology (Kellerhals and Bray, 1971), and it is based on picking clasts at the nodes of a regular grid. In this study the method was applied on high-resolution orthophotos (0.5 m pixel size) by manually mapping the single blocks at the nodes of a 10,000 m^2 grid with 10x10 m cell size (i.e., 100 blocks from each grid) (see Supplementary Figure 2).
To evaluate the frequency distribution associated with each lithology, the exceedance relative frequency of the block volume has been reported (Fig. 14). The analysis of these volume frequency distributions reveals a power-law behaviour for values greater than some minimum volume, with a roll-over for smaller volumes probably due to undersampling, and a truncation at 0.1 m^3, corresponding to the limit of the orthophoto resolution.

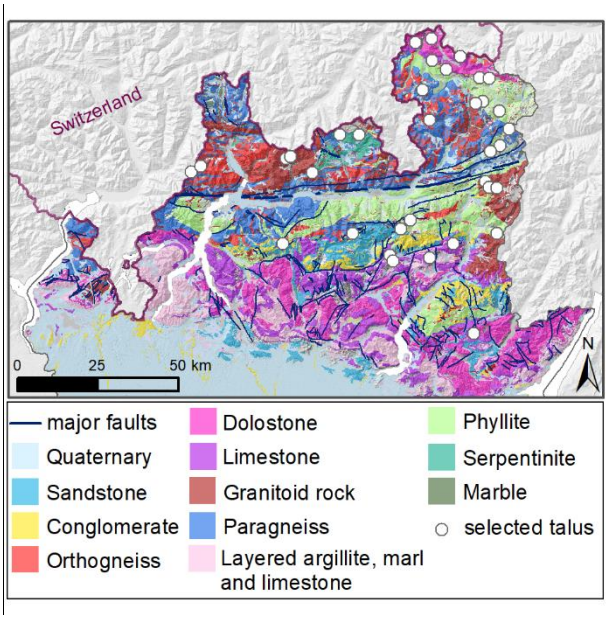

Fig. 13 *Lithological map obtained by reclassification of the 1:250.000 scale Geological map of Lombardy. White points stand for the selected talus where the block volume analysis has been carried out.*

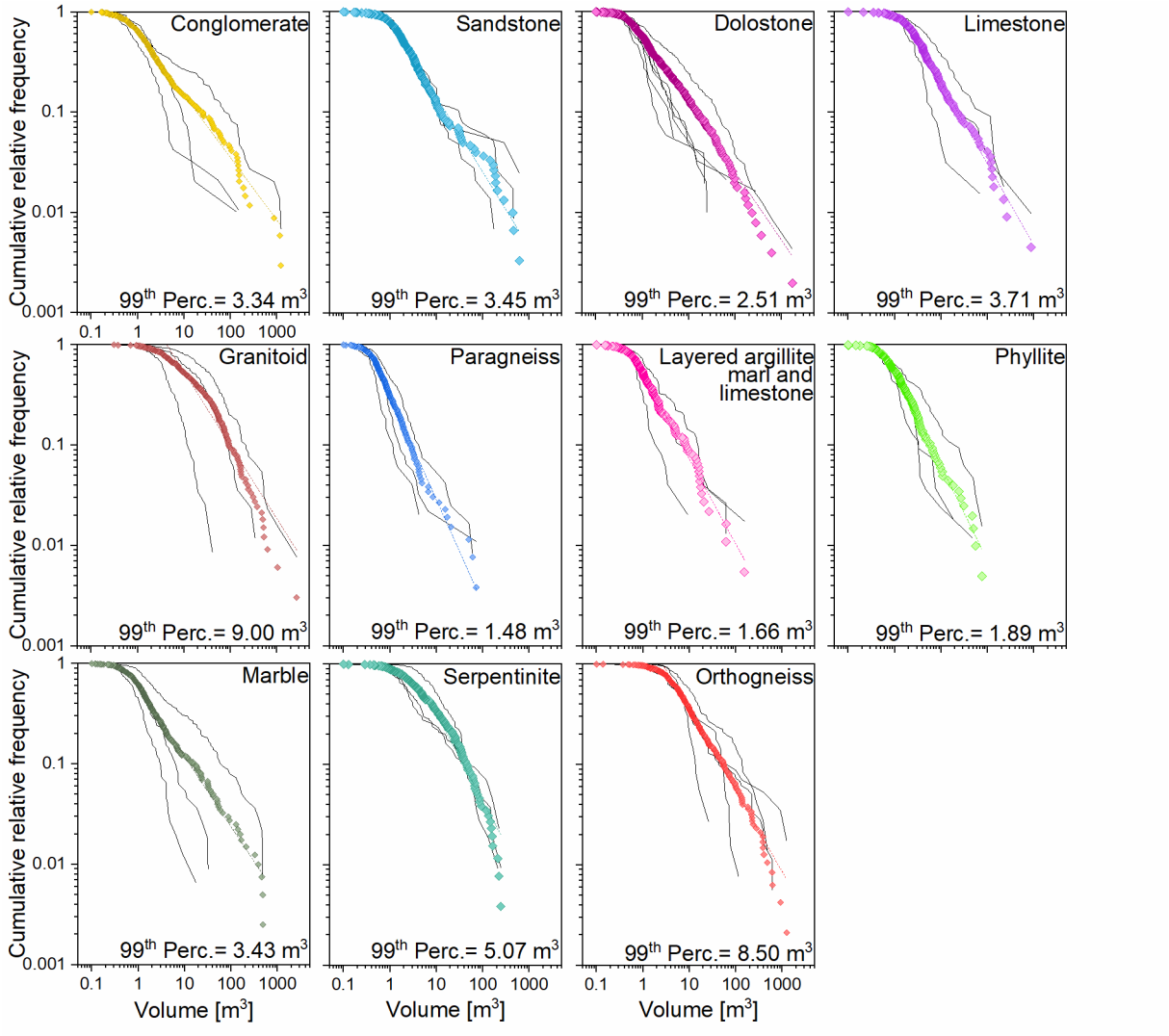

Fig. 14 *Cumulative relative frequency distribution of the blocks volume for each examined lithology. The different black curves in each graph represent the different talus analysed for each lithological class (coloured lines). The absence of values under 0.1 m³ is related to the limit in resolution of the used photos.*

The power-law exponent has been compared with the literature, showing a good agreement with values reported by Ruiz et al. (2017) for limestone, schist, sandstone and conglomerate (Table 4). The exponent for granitoid is greater, probably due to the fact that Dussauge et al. (2003) analysed the detached volume from rock masses whereas we focus on the blocks already on the ground, thus ignoring the larger fragmented blocks and shifting our exponent.

Table 4 *Comparison between the exponents of the fitted cumulative power-law relationships reported in the literature and the ones obtained in this study.*

	Power law exponent		
lithology	**literature**	**this study**	**R^2** (this study)
Limestone	0.72-1.27 (1) (2)	0.82	0.99
Schist	0.92 (1)	0.94	0.99
Granitoid	0.45 (2)	1.10	0.99
Sandstone	0.51-0.53 (1)	0.75	0.99
Conglomerate	0.74 (1)	0.63	0.99
Dolostone	-	0.69	0.99
Layered argillite, marl and limestone	-	0.85	0.99
Marble	-	0.70	0.99
Orthogneiss	-	0.83	0.99
Paragneiss	-	1.04	0.99
Serpentinite	-	1.29	0.96

(1) Ruiz et al, 2017; (2) Dussauge et al., 2003

Due to the impossibility to identify a characteristic volume for each lithological class starting from a power-law (scale invariant) distribution (Hovius et al. 1997; Pelletier et al. 1997; Hovius et al. 2000; Stark and Hovius 2001; Malamud et al. 2004; Frattini and Crosta 2013), we extracted different percentiles of the volume. To calculate this percentiles, we added to the distribution the blocks with volume smaller than 0.1 m^3 that were not visible from the othophotos in correspondence to the nodes of a 10,000 m^2 grid with 10x10 m cell size. For some lithologies (e.g., limestone), these unknown blocks amount to almost 85% of the total blocks, making impossible to correctly determine percentiles smaller than the 85th. The effect of selecting different percentiles percentile for the calculation of the EEI is shown in figure 15b, where the cumulative distribution of the EEI values for Lombardy Region forest is illustrated. Following a conservative approach, we decided to adopt the 99th to produce the map of the protective forests efficiency (Fig. 15). With this percentile, the extent of protection forests with an EEI greater than 0.5 amounts to 5124 km^2, approximately 67% of the total protection forests (Fig 15b). Most of the low efficiency forests (< 0.1) are placed at the end of the slopes just before the inhabited areas, since these are usually the weakest forest types (i.e. broadleaf forests), and the smallest forest polygons because changes in forest types occur close to residential zones and valley bottom.

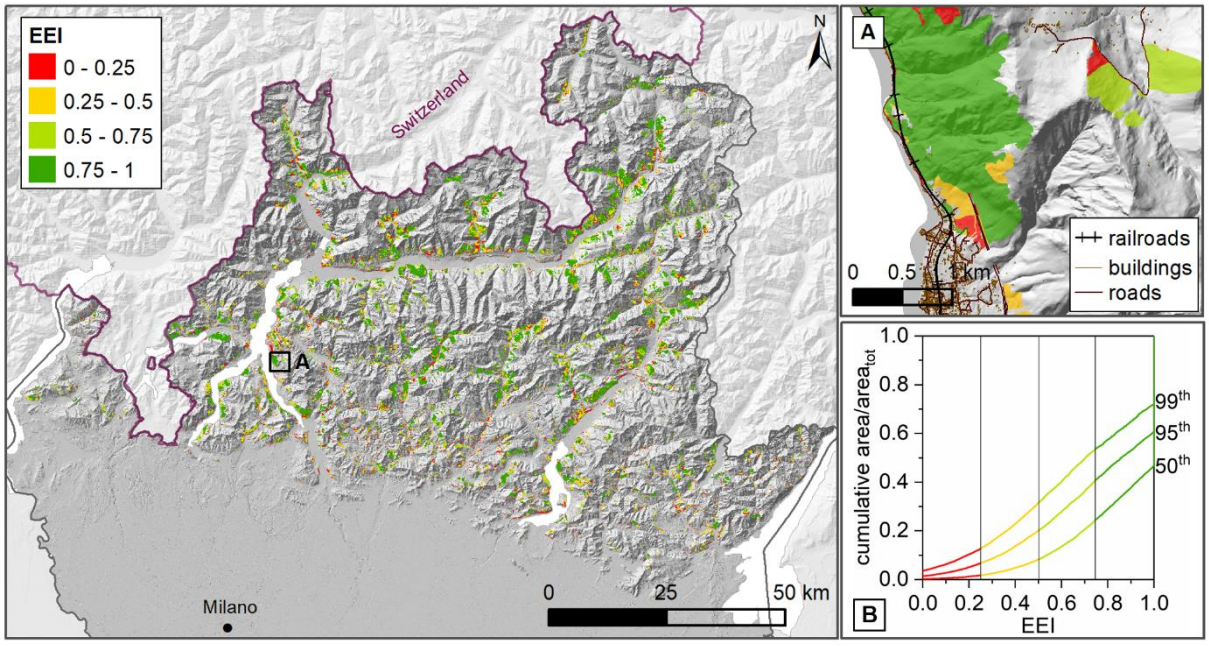

Fig. 15 *Map of the protective forests classified according to the EEI index calculated by using the 99th percentile of the block volumes cumulative distribution. A) inset of the EEI index map, with the elements at risks. B) Cumulative distribution of the EEI values, obtained from the regression model by using the 50th, 95th, and 99th percentiles of the cumulative frequency-volume distribution.*

Discussion

The role and capability of rockfall protection forests at mitigating rockfall hazard and risk has been recognized in many areas. Nevertheless, very little has been done to quantify the effects of rockfall protection forests except for very local scale studies. Three main issues need to be tackled and discussed:

1- the identification and mapping of rockfall protection forests at regional scale;

2- the efficiency of different protection forests;

3- the controlling parameters on the forest efficiency.

Regional mapping identification of protection forests

The main limitations of the proposed methodology for the identification and mapping at regional scale of the Rockfall Protection Forests (RPForest) are: the need for a post-processing visual check of identified areas, and the assessment of rockfall onset susceptibility. The visual check is required in areas with hairpin roads (in these cases we can not only compare the average elevation of forest and the median elevation of the road because this would identify only the area above the highest hairpin turn as a protective forest) or with rivers

interposed between the rockfall area and the element at risk (the river cancelling the risk for that element). To identify all the Rockfall Protection Zone (RPZone) and all the Rockfall Protection Forests (RPForest), we needed to simulate worst-case rockfall scenarios. These scenarios were modelled in HY-STONE assuming a rockfall onset susceptibility everywhere equal to 1. This strong assumption involves simplified rockfall models, but it was necessary due to the regional working scale and to the aim of identifying every potential RPZone and RPForest from a conservative perspective.

The proposed methodology, despite these criticalities, is reliable and applicable at regional scale, although it would require a detailed in situ visual check of the RPForest.

A comparison between the RPForest and the protection forests identified and mapped at local scale by forest management technicians in 1975 (1975_PForests) was carried out in a sample area of the Lombardy Region (Fig. 16). The 1975_PForests are characterized by a smaller extent for two main reasons: (i) the mapping was performed at a local scale for specific elements at risk after the occurrence of different types of natural phenomena (e.g. rockfalls, shallow landslides, debris flows, snow avalanches, and windstorms; as defined by the 1926 Italian Royal Decree); (ii) the forest extent was smaller with respect to the present day conditions (Fig. 16).

Before the application of the proposed methodology, different attempts were accomplished to define the best approach to identify the rockfall protection forests (Fig. 17). By using a method based only on the most-likely scenario (i.e. calibrated restitution coefficients), the trajectories frequently stopped at short distance (i.e. few tens of meters) from the elements at risk (Fig. 17a). In such cases, a small uncertainty in the definition of the source areas, the slope geometry, or the restitution coefficients could result in a shift of the rockfall area, thus affecting the elements at risk. To overcome this issue, a buffer zone of few tens of meters could be applied to the rockfall extent polygons, but this would cause spurious intersections with elements at risk located on the slope laying beyond the ridge (Fig. 17b). Another method, based on the combination of rockfall modelling (i.e. trajectories) and hydrogeological approach (i.e. hydrologically contributing area upstream of each element at risk) generated an exaggeration in the polygon's extent, with the identification of forests that do not protect element at risks directly (Fig. 17c).

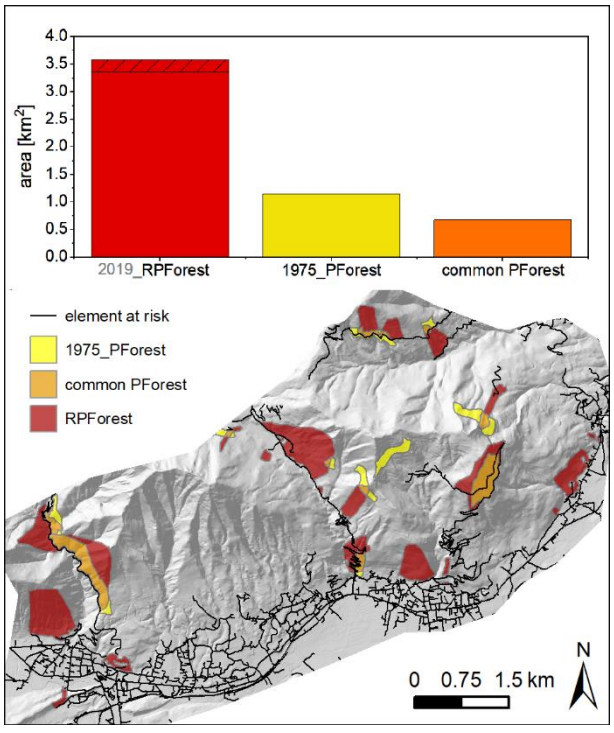

Fig. 16 *Comparison between the Rockfall Protection Forests (RPForest, red polygons) and the protection forests mapped at local scale in 1975 (1975_PForests yellow polygons). The comparison is shown for a small area for which both datasets are available. "Common PForest" refers to areas classified as protection forest in both datasets. Part of the 2019 RPForest area is associated to an increase in forest extent from 1975 to 2019 (see the upper hatched portion of the 2019 RPForest bar).*

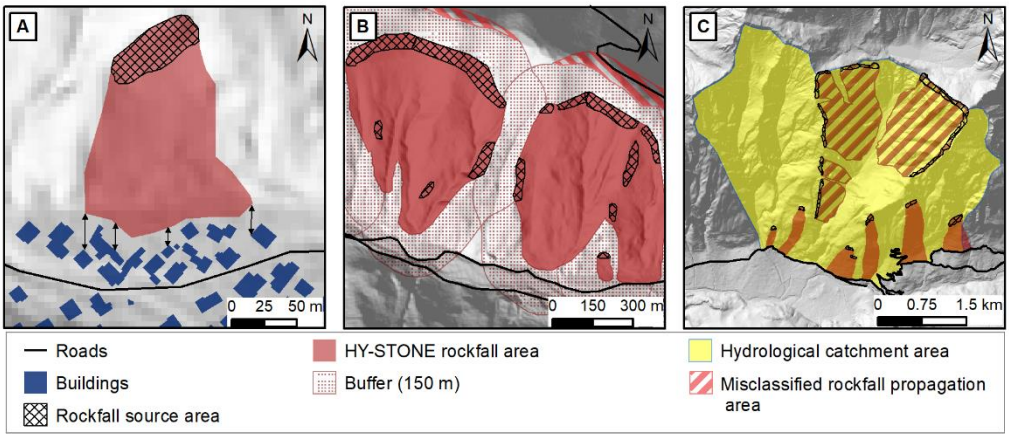

Fig. 17 *Examples of problems in semi-automatic mapping of rockfall protection forests. a) Lack of intersection between rockfall extent areas and the elements at risk by a very short distance, as indicated by the arrows. b) Tentative solution to problem (a) by the generation of a 100 m buffer zone around the rockfall extent area. This caused the mapping of invasion areas beyond the mountain ridge, wrongly intersecting elements at risk on the opposite mountain slope. c) Use of the hydrological approach, which caused the mapping of false protection forests within the catchment where the elements at risk do not exist.*

Efficiency of protection forest types

The efficiency of different forest types was assessed by empirical and modelling approaches.

The empirical approach shows an increase of the energy line angle from about 36° for non-forested slopes to over 40° for forested slopes. With respect to the literature (Lied 1977; Onofri and Candian 1979; Meissl 1998; Dorren et al. 2005; Copons et al. 2009) these values are, on average, greater both for forested and non-forested slopes. This may be due to the fact that the angle has been estimated along a straight line and not along the actual rockfall path, and maybe due to valley morphology constraints for some of the rockfall events (Frattini et al. 2012). In addition, the empirical approach applied at regional scale is affected by several uncertainties, such as: 1) the energy-line analysis assigns the angle to the forest type that has the longest extent along the energy line profile. Therefore, it is possible that the angle is affected by the effect of other forests types along the path; 2) the forest cover map used for the energy line analysis corresponds to the current land cover, which may have been different for old rockfall events; 3) the presence of mitigation measures (e.g. catch nets, embankments and ditches) installed close to inhabited areas, can lead to an incorrect (but conservative) energy-line angle.

For the analysis of the efficiency with the modelling approach, we propose in this paper a new efficiency index (EEI) based on the AUC of the kinetic energy as a function of distance. This index integrates the rockfall energy reduction due to the forest damping effect along the entire forested slope section. We suggest this approach being more meaningful for forest efficiency quantification with respect to the analysis of runout distance percentiles, as usually done in the literature (Dupire et al. 2016 and Moos et al. 2017). Overall, the modelling approach allows quantitative efficiency assessment by simulating actual forest characteristics, overcoming empirical approach simplifications and approximations linked to historical events data collection. However, the use in this analysis of average forests parameters for the different forest types (i.e., mean values of DBH and of forest density) is not fully realistic because it does not take into account forest diversity, heterogeneity, and maturity.

Controlling parameters: the role of lithology

The sensitivity analysis demonstrates that the block diameter, slope inclination, DBH of trees and forest density are, in decreasing order of relevance, the most important sensitive parameters (Fig. 12). Therefore, estimating the expected volume for each (macro) lithological class is essential since the efficiency can decrease drastically, when higher volumes are considered. The regional-scale strategy for block-volume estimation based on the analysis of talus grain size from orthophotos involves a few weaknesses: (i) the resolution of the orthophotos does not allow to recognize blocks smaller than approximately 0.2 m^3, resulting in an under-sampling of smaller blocks, partially solved by using a truncation of the distribution of about 0.1 m^3; (ii) the point-sampling method causes an over-sampling of larger blocks due to their greater probability of intersection with the sampling points compared to smaller blocks, solved by weighting the frequency by the inverse of the area occupied by the block; (iii) smaller blocks may show larger dimensions due to the difficulty of contouring their shape.

Despite these critical issues, our block mapping strategy satisfies the purpose, also considering the regional scale of the analysis, although it would require a strong future implementation. Moreover, the undersampling of smaller block, which are difficult to map on orthophotos (smaller than 0.2 m^3), does not affect significantly the calculation of the forest efficiency that is always very high for small blocks. For instance, for the ManHorn forest type (Fig. 12), which is an average-efficient forest type, EEI is already greater than 0.95 when block radius is smaller than 0.4 m (i.e. spherical volume of 0.27 m^3), and greater than 0.99 when block radius is smaller than 0.25 m (i.e. spherical volume of 0.07 m^3) (Fig. 12).
The statistical analysis of the EEI index frequency distributions of Lombardy-region forests for different lithologies (Fig. 16) confirms the importance of block size (larger than 0.2 m^3). Forests that lay below rockfall sources characterized by larger block volumes (e.g. granitoid and orthogneiss rocks) show the highest frequencies of low efficiency values (<0.1), while those in areas characterized by smaller block volumes (e.g. paragneiss and phyllite rocks) show a more uniform frequency distribution.

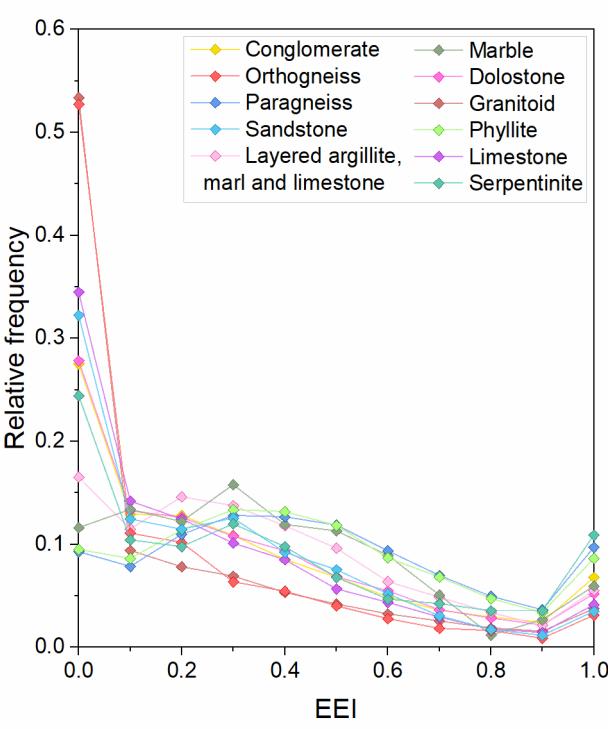

Fig. 18 *Statistical analysis of EEI frequency distribution for different lithologies.*

Conclusions

This study presents a successful methodology to map rockfall protection forests at the regional scale by using a semi-automatic GIS-based method, and to achieve quantitative evaluation of protection forest efficiency, considering site specific forest, morphological and lithological parameters. With respect to the empirical runout models based on the energy line concept, the use of 3D simulation models such as HY-STONE goes well beyond the limitations of the shadow angle approach, taking into account the geomorphological setting of each slope sector along the rockfall path and simulating realistic trajectories. The presented methodology to define protection forests solves the uncertainties connected to the definition of rockfall propagation areas, overcoming the limitations of the hydrological approach.
The new forest protection efficiency index, EEI, proposed in this paper allows to quantify the protection efficiency of forest in terms of kinetic energy reduction. This index provides a single-value measure of efficiency that is suitable for regional scale mapping.
Among the parameters controlling the efficiency, we highlight the importance of a non-forest parameter such as the expected volume of the blocks. This volume mainly depends on local-scale rock-mass structure and it is impossible to forecast accurately at a regional scale. To tackle such a problem, we applied a new approach, which is based on the analysis of debris talus form orthophotos. This approach demonstrated to be suitable to explore the regional-scale dependence of the expected block volume on lithology for the efficiency mapping of protection forest.
This research allowed to produce a new regional-scale map of protective forests for Lombardy Region also considering an EEI index, which quantifies the actual expected efficiency of each individual forest. This map

is a new tool for a reliable regional-scale forest management in the light of rockfall protection and hazard zonation.

Acknowledgements

The research has been funded by: the RockTheAlps INTERREG III project, the CARIPLO 2016-0756—@RockHoRiZon—Advanced Tools for Rockfall Hazard and Risk zonation at the Regional Scale, and the Project MIUR-Dipartimenti di Eccellenza 2018–2022. The forest data was provided by Bruna Comini, Dario Lombardi and Martino Gambacorti from ERSAF and Emanuele Lingua from the University of Padova. The authors also wish to thank Paolo Visentin and Elena Valbuzzi from the University of Milano Bicocca, Mauro Masiero and Giulia Amato from Etifor srl.

References

Agliardi F, Crosta GB (2003) High resolution three-dimensional numerical modelling of rockfalls. International Journal of Rock Mechanics and Mining Sciences 40(4):455-471

Azzoni A, La Barbera G, Zaninetti A (1995) Analysis and prediction of rockfalls using a mathematical model. International journal of rock mechanics and mining sciences & geomechanics abstracts. 32 (7). Pergamon

Berger F, Quetel C, Dorren LK (2002) Forest: a natural protection mean against rockfalls, but with which efficiency. In International congress INTERPRAEVENT (Vol. 2, pp. 815-826)

Berger F, Dorren LK (2007) Principles of the tool Rockfor. Net for quantifying the rockfall hazard below a protection forest. Schweizerische Zeitschrift fur Forstwesen 158(6):157-165

Bigot C, Dorren LK, Berger F (2009) Quantifying the protective function of a forest against rockfall for past, present and future scenarios using two modelling approaches. Natural hazards 49(1):99-111

Brauner M, Weinmeister W, Agner P, Vospernik S, Hoesle B (2005) Forest management decision support for evaluating forest protection effects against rockfall. Forest Ecology and Management 207(1-2):75-85

Bourrier F, Dorren LK, Nicot F, Berger F, Darve F (2009) Toward objective rockfall trajectory simulation using a stochastic impact model. Geomorphology 110(3-4):68-79

Chau KT, Wong RHC, Liu J, Lee CF (2003) Rockfall hazard analysis for Hong Kong based on rockfall inventory. Rock Mechanics and Rock Engineering 36(5):383-408

Copons R, Vilaplana JM, Linares R (2009) Rockfall travel distance analysis by using empirical models (Sola d'Andorra la Vella, Central Pyrenees). Natural Hazards & Earth System Sciences 9:2107–2118

Crosta GB, Agliardi F (2003) A methodology for physically based rockfall hazard assessment. Natural Hazards and Earth System Science 3:407–422

Crosta GB, Agliardi F (2004) Parametric evaluation of 3D dispersion of rockfall trajectories. Natural Hazards and Earth System Science 4:583-598

Crosta GB, Agliardi F, Frattini P, Lari S (2015) Key issues in rockfall modelling, hazard and risk assessment for rockfall protection. In Engineering Geology for Society and Territory 2:43-58. Springer, Cham.

Delonca A, Gunzburger Y, Verdel T (2014) Statistical correlation between meteorological and rockfall databases. Natural Hazards and Earth System Sciences, 14(8), 1953-1964.

Di Prisco C, Vecchiotti M (2006) A rheological model for the description of boulder impacts on granular strata. Geotechnique 56:469-482

Dorren LK, Seijmonsbergen AC (2003) Comparison of three GIS-based models for predicting rockfall runout zones at a regional scale. Geomorphology 56 (1-2):49-64

Dorren LK, Berger F, Imeson AC, Maier B, Rey F (2004a) Integrity, stability and management of protection forests in the European Alps. Forest ecology and management 195(1-2):165-176

Dorren LK, Berger F, Le Hir C, Mermin E, Tardif P (2005) Mechanisms, effects and management implications of rockfall in forests. Forest Ecology and Management 215(1-3):183-195

Dorren LK, Berger F, (2006) Stem breakage of trees and energy dissipation during rockfall impacts. Tree physiology 26(1): 63-71.

Dorren LK, Berger F, Putters US (2006) Real-size experiments and 3-D simulation of rockfall on forested and non-forested slopes. Natural Hazards and Earth System Sciences 6:145-153

Douglas GR (1980) Magnitude frequency study of rockfall in Co. Antrim, N. Ireland. Earth Surface Processes 5(2):123-129

Dupire S, Bourrier F, Monnet JM, Bigot S, Borgniet L, Berger F, Curt T (2016) Novel quantitative indicators to characterize the protective effect of mountain forests against rockfall. Ecological indicators 67:98-107

Dussauge C, Grasso JR, Helmstetter A (2003) Statistical analysis of rockfall volume distributions: Implications for rockfall dynamics. Journal of Geophysical Research: Solid Earth 108(B6)

Elkin C, Gutiérrez AG, Leuzinger S, Manusch C, Temperli C, Rasche L, Bugmann H (2013) A 2° C warmer world is not safe for ecosystem services in the European Alps. Global Change Biology 19(6):1827-1840

Evans SG, Hungr O (1993). The assessment of rockfall hazard at the base of talus slopes. Canadian Geotechnical journal 30(4):620-636

Frattini P, Crosta G, Ceriani M, Fossati D (2003) Inventario delle frane e dei dissesti della regione Lombardia: analisi statistica e probabilistica per una valutazione preliminare della pericolosità. In I convegno nazionale AIGA, 427-448. Rendina Editore

Frattini P, Crosta G, Carrara A, Agliardi F (2008) Assessment of rockfall susceptibility by integrating statistical and physically-based approaches. Geomorphology 94(3-4):419-437

Frattini P, Crosta GB, Agliardi F (2012) Rockfall characterization and modeling. Landslides: types, mechanisms and modelling 22:267-281

Frattini P, Crosta GB, Agliardi F, Imposimato S (2013) Challenging calibration in 3D rockfall modelling. In Landslide science and practice, 169-175. Springer, Berlin, Heidelberg

Gasparini P, Tabacchi G (2011) L'Inventario Nazionale delle Foreste e dei serbatoi forestali di Carbonio INFC 2005. Secondo inventario forestale nazionale italiano. Metodi e risultati. Ministero delle Politiche Agricole, Alimentari e Forestali 653

Gehrig-Fasel J, Guisan A, Zimmermann NE (2007) Tree line shifts in the Swiss Alps: climate change or land abandonment?. Journal of Vegetation Science 18:571-582
Guzzetti F, Crosta G, Detti R, Agliardi F (2002) STONE: a computer program for the three-dimensional simulation of rockfalls. Computers & Geosciences 28(9):1079-1093
Hovius N, Stark CP, Allen PA (1997) Sediment flux from a mountain belt derived by landslide mapping. Geology 25(3):231-234
Hovius N, Stark CP, Hao-Tsu C, Jiun-Chuan L (2000) Supply and removal of sediment in a landslide-dominated mountain belt: Central Range, Taiwan. The Journal of Geology 108(1):73-89
Innocenzi E, Greggio L, Frattini P, de Amicis M (2017) A Web-Based Inventory of Landslides Occurred in Italy in the Period 2012–2015. In Workshop on World Landslide Forum 1127-1133. Springer, Cham.
Jaboyedoff M, Labiouse V (2003) Preliminary assessment of rockfall hazard based on GIS data. 10th ISRM Congress. International Society for Rock Mechanics and Rock Engineering
Jahn J (1988) Entwaldung und Steinschlag. Interpraevent Proceedings, Graz. Tagungspubl. 1:185-198. In German with English abstract
Jancke O, Dorren LK, Berger F, Fuhr M, Köhl M (2009) Implications of coppice stand characteristics on the rockfall protection function. Forest ecology and management 259(1):124-131
Kajdiž P, Diaci J, Rebernik J, (2015) Modelling facilitates silvicultural decision-making for improving the mitigating effect of beech (Fagus sylvatica L.) dominated alpine forest against rockfall. Forests 6(6):2178-2198
Leine RI, Schweizer A, Christen M, Glover J, Bartelt P, Gerber W (2014) Simulation of rockfall trajectories with consideration of rock shape. Multibody System Dynamics 32(2):241-271
Lied K (1977) Rockfall problems in Norway. ISMES Publication 90:51-53
Malamud BD, Turcotte DL, Guzzetti F, Reichenbach P (2004) Landslide inventories and their statistical properties. Earth Surface Processes and Landforms 29(6):687-711
Marazzi S (2005) Atlante orografico delle Alpi. SOIUSA. Suddivisione orografica internazionale unificata del Sistema Alpino. Quaderni di cultura alpina. Priuli & Verlucca. In Italian
Macciotta R, Hendry M, Cruden DM, Blais-Stevens A, Edwards T (2017) Quantifying rockfall probabilities and their temporal distribution associated with weather seasonality. Landslides 14(6):2025-2039
Meißl G (1998) Modellierung der Reichweite von Felsstürzen: Fallbeispiele zur GIS-gestützten Gefahrenbeurteilung aus dem Bayerischen und Tiroler Alpenraum; mit 24 Tabellen. Selbstverl. d. Inst. für Geographie d. Univ.
Moos C, Fehlmann M, Trappmann D, Stoffel M, Dorren LK (2018) Integrating the mitigating effect of forests into quantitative rockfall risk analysis–Two case studies in Switzerland. International journal of disaster risk reduction 32:55-74
Moos C, Dorren L, Stoffel M (2017) Quantifying the effect of forests on frequency and intensity of rockfalls. Natural Hazards and Earth System Sciences 17(2):291-304
Moya J, Corominas J, Arcas JP, Baeza C (2010) Tree-ring based assessment of rockfall frequency on talus slopes at Solà d'Andorra, Eastern Pyrenees Geomorphology 118(3-4):393-408
Onofri R, Candian C (1979) Indagine sui limiti di massima invasione dei blocchi rocciosi franati durante il sisma del Friuli del 1976. Reg. Aut. Friuli–Venezia Giulia, Cluet.
Pelletier JD, Malamud BD, Blodgett T, Turcotte DL (1997) Scale-invariance of soil moisture variability and its implications for the frequency-size distribution of landslides. Engineering Geology 48(3-4):255-268
Perret S, Dolf F, Kienholz H (2004) Rockfalls into forests: analysis and simulation of rockfall trajectories - considerations with respect to mountainous forests in Switzerland. Landslides 1(2):123-130
Perret S, Baumgartner M, Kienholz H (2006) Inventory and analysis of tree injuries in a rockfall-damaged forest stand. European journal of forest research 125(2):101-110
Pfeiffer TJ, Bowen TD (1989) Computer simulation of rockfalls. Bulletin of the association of Engineering Geologists 26(1):135-146
Radtke A, Toe D, Berger F, Zerbe S, Bourrier F (2014) Managing coppice forests for rockfall protection: lessons from modeling. Annals of forest science 71(4):485-494
Rammer W, Brauner M, Dorren LK, Berger F, Lexer MJ (2010) Evaluation of a 3-D rockfall module within a forest patch model. Natural Hazards and Earth System Sciences 10(4), p-699
Regione Lombardia (1987) Base informativa della cartografia Geoambientale - Carta litologica. Available at http://www.geoportale.regione.lombardia.it (Accessed 26 September 2019)
Regione Lombardia (2012) Uso e copertura del suolo 2012 (DUSAF 4.0. Available at http://www.geoportale.regione.lombardia.it (Accessed 26 September 2019)
Regione Lombardia (2014) DTM 20 - ESRI GRID. Available at http://www.geoportale.regione.lombardia.it (Accessed 26 September 2019)
Regione Lombardia (2015) DTM 5X5 - Modello digitale del terreno (ed. 2015. Available at http://www.geoportale.regione.lombardia.it (Accessed 26 September 2019)
Ruiz-Carulla R, Corominas J, Mavrouli O (2017) A fractal fragmentation model for rockfalls. Landslides 14(3):875-889

Sass O, Oberlechner M (2012) Is climate change causing increased rockfall frequency in Austria? Natural Hazards and Earth System Sciences 12(11):3209-3216
Schneuwly DM, Stoffel M (2008) Tree-ring based reconstruction of the seasonal timing, major events and origin of rockfall on a case-study slope in the Swiss Alps. Natural Hazards and Earth System Sciences 8(2):203-211
Šilhán K, Pánek T, Hradecký J (2013) Implications of spatial distribution of rockfall reconstructed by dendrogeomorphological methods. Natural Hazards and Earth System Sciences 13(7):1817-1826
Stark CP, Hovius N (2001) The characterization of landslide size distributions. Geophysical Research Letters 28(6):1091-1094
Stoffel M, Lièvre I, Monbaron M, Perret S (2005) Seasonal timing of rockfall activity on a forested slope at Täschgufer (Swiss Alps) – a dendrochronological approach. Zeitschrift für Geomorphologie 89-106
Stoffel M, Schneuwly D, Bollschweiler M, Lievre I, Delaloye R, Myint M, Monbaron M (2005) Analyzing rockfall activity (1600–2002) in a protection forest—a case study using dendrogeomorphology. Geomorphology 68(3-4):224-241
Stoffel M, Wehrli A, Kühne R, Dorren LK, Perret S, Kienholz H (2006) Assessing the protective effect of mountain forests against rockfall using a 3D simulation model. Forest Ecology and Management 225(1-3):113-122
Stokes A, Salin F, Kokutse AD, Berthier S, Jeannin H, Mochan S, Fourcaud T (2005) Mechanical resistance of different tree species to rockfall in the French Alps. Plant and soil 278(1-2):107-117
Tanarro LM, Muñoz J (2012) Rockfalls in the Duraton canyon, central Spain: Inventory and statistical analysis. Geomorphology 169:17-29
Toe D, Mentani A, Govoni L, Bourrier F, Gottardi G, Lambert S (2018) Introducing meta-models for a more efficient hazard mitigation strategy with rockfall protection barriers. Rock mechanics and rock engineering 51(4):1097-1109
Trigila A, Iadanza C, Spizzichino D (2010) Quality assessment of the Italian Landslide Inventory using GIS processing. Landslides 7(4):455-470
Wieczorek GF, Snyder JB, Alger CS, Isaacson KA (1992) Yosemite historical rockfall inventory. US Geol. Surv. Open File Report 38:92-387
Whitman MS, Moran EH, Ourso RT (2003) Photographic techniques for characterizing streambed particle sizes. Transactions of the American Fisheries Society 132(3):605-610
Wolman MG (1954) A method of sampling coarse river-bed material. Transactions of the American Geophysical Union 35:951–956

Supplementary

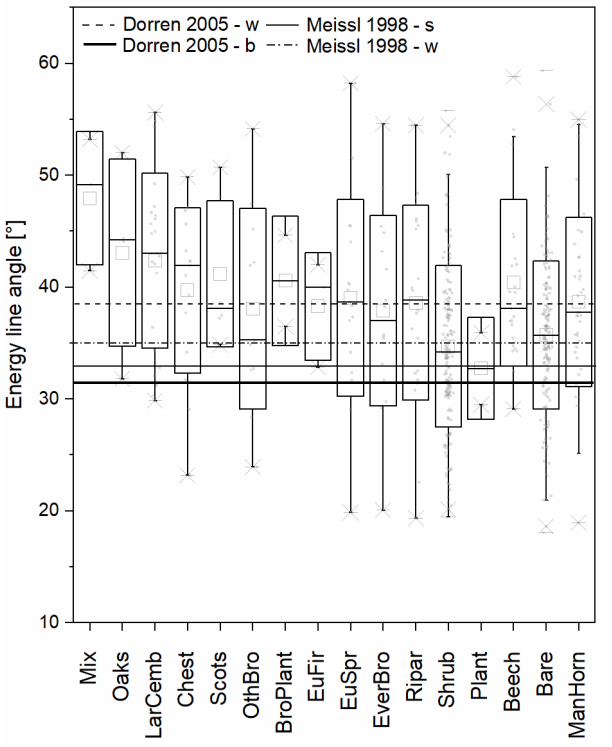

Supplementary Figure 1 Energy line angle distributions of the forest type of the rockfall polygons. In this figure, only those rockfalls that completely fall within a single forest type are considered. The different lines represent energy line reported in literature. For forested area Meissl (1998) proposed an energy line value of 35° (dash dot line -w), while Dorren et al. (2005) suggested a value of 38° (dashed line - w). For bare and shrub areas, a 32° and 33° value respectively have been proposed by Dorren et al. (2005)(thick continuous line, -b) and Meissl (1998) (continuous line, -s).

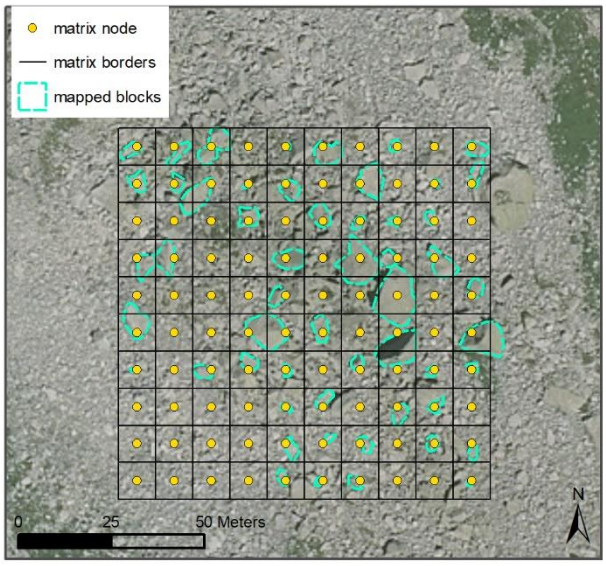

Supplementary Figure 2 The sampling method applied on high-resolution orthophotos of analysed talus, based on manually mapping the single blocks at the nodes of a 10,000 m2 grid with 10x10 m cell size.

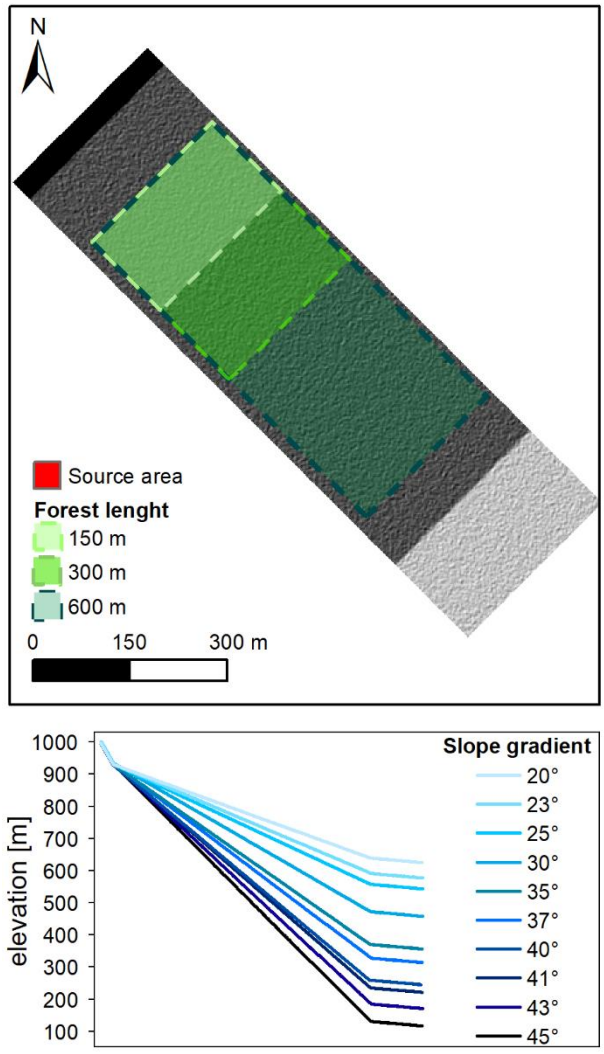

Supplementary Figure 3 The 1000 m-long synthetic slope used in SC_PAR simulations. Examples of forests with different lengths simulated in HY-STONE are reported in green. The slope has three different sectors: a 40 m-long steep sector with an inclination of 60°, an 800 m-long sector with variable inclination (20° to 45°), and a bottom flat sector with an inclination of 5°. The rockfall source area has been positioned on the top of the steep sector.

Supplementary Table 1 Parametric simulations strategy. In bold, the values of the modified parameters.

simulation	FLU types	DBH [m]	tree density [n°trees/ha]	slope gradient [°]	forest length [m]	forest position (distance from source area) [m]	block radius [m]	*EEI*
SC_FOR1	LarCemb	0.220	842.2	30	350	250	0.5	0.94
SC_FOR2	EuSpr	0.270	856.4	30	350	250	0.5	0.97
SC_FOR3	EuFir	0.260	1062.0	30	350	250	0.5	0.98
SC_FOR4	Scots	0.170	1275.5	30	350	250	0.5	0.88
SC_FOR5	MixCon	0.200	1114.0	30	350	250	0.5	0.94
SC_FOR6	Beech	0.180	1198.6	30	350	250	0.5	0.96
SC_FOR7	Oaks	0.150	1159.2	30	350	250	0.5	0.76
SC_FOR8	Chest	0.200	1169.0	30	350	250	0.5	0.94
SC_FOR9	ManHorn	0.110	1856.2	30	350	250	0.5	0.58
SC_FOR10	Ripar	0.190	924.4	30	350	250	0.5	0.84
SC_FOR11	OthBro	0.150	1456.4	30	350	250	0.5	0.94
SC_FOR12	EverBro	0.120	1663.0	30	350	250	0.5	0.88
SC_FOR13	BlackPop	0.230	298.5	30	350	250	0.5	0.09
SC_FOR14	BroPlant	0.100	395.1	30	350	250	0.5	0.94
SC_FOR15	Mix	0.190	1048.2	30	350	250	0.5	0.80
SC_FOR16	Beech	0.180	1198.6	30	350	250	0.6	0.80
SC_FOR17	LarCemb	0.220	842.2	30	350	250	0.6	0.63
SC_FOR18	EuSpr	0.270	856.4	30	350	250	0.6	0.87
SC_FOR19	EuFir	0.260	1062.0	30	350	250	0.6	0.89
SC_FOR20	Scots	0.170	1275.5	30	350	250	0.6	0.35
SC_FOR21	MixCon	0.200	1114.0	30	350	250	0.6	0.54
SC_FOR22	Oaks	0.150	1159.2	30	350	250	0.6	0.46
SC_FOR23	Chest	0.200	1169.0	30	350	250	0.6	0.89
SC_FOR24	ManHorn	0.110	1856.2	30	350	250	0.6	0.23
SC_FOR25	Ripar	0.190	924.4	30	350	250	0.6	0.10
SC_FOR26	OthBro	0.150	1456.4	30	350	250	0.6	0.58
SC_FOR27	EverBro	0.120	1663.0	30	350	250	0.6	0.38
SC_FOR28	BlackPop	0.230	298.5	30	350	250	0.6	0.05
SC_FOR29	BroPlant	0.100	395.1	30	350	250	0.6	0.54
SC_FOR30	Mix	0.190	1048.2	30	350	250	0.6	0.56
SC_SENS31	ManHorn	0.110	1860.0	30	300	275	**0.3**	0.92
SC_SENS32	ManHorn	0.110	1860.0	30	300	275	**0.5**	0.57
SC_SENS33	ManHorn	0.110	1860.0	30	300	275	**1.0**	0.21
SC_SENS34	ManHorn	0.110	1860.0	30	**150**	150	0.5	0.44
SC_SENS35	ManHorn	0.110	1860.0	30	**600**	150	0.5	0.69
SC_SENS36	ManHorn	0.110	1860.0	30	300	**137.5**	0.5	0.56
SC_SENS37	ManHorn	0.110	1860.0	30	300	**550**	0.5	0.53
SC_SENS38	ManHorn	0.110	**930.0**	30	300	275	0.5	0.20
SC_SENS39	ManHorn	0.110	**3720.0**	30	300	275	0.5	0.75
SC_SENS40	ManHorn	**0.060**	1860.0	30	300	275	0.5	0.07
SC_SENS41	ManHorn	**0.230**	1860.0	30	300	275	0.5	0.99

SC_SENS42	ManHorn	0.110	1860.0	**20**	300	275	0.5	1.00
SC_SENS43	ManHorn	0.110	1860.0	**25**	300	275	0.5	0.97
SC_SENS44	ManHorn	0.110	1860.0	**35**	300	275	0.5	0.38
SC_SENS45	ManHorn	0.110	1860.0	**40**	300	275	0.5	0.34
SC_SENS46	ManHorn	0.110	1860.0	**23**	300	275	0.5	0.94
SC_SENS47	ManHorn	0.110	1860.0	**37**	300	275	0.5	0.26
SC_SENS48	ManHorn	0.110	1860.0	**41**	300	275	0.5	0.23
SC_SENS49	ManHorn	0.110	1860.0	**43**	300	275	0.5	0.21
SC_SENS50	ManHorn	0.110	1860.0	**45**	300	275	0.5	0.19
SC_SENS51	ManHorn	0.110	1860.0	30	300	275	**0.4**	0.98
SC_SENS52	ManHorn	0.110	1860.0	30	300	275	**0.4**	0.95
SC_SENS53	ManHorn	0.110	1860.0	30	300	275	**0.6**	0.23
SC_SENS54	ManHorn	0.110	1860.0	30	300	275	**0.8**	0.11
SC_SENS55	ManHorn	0.110	1860.0	30	300	275	**0.8**	0.10
SC_SENS56	ManHorn	0.110	1860.0	30	300	275	**1.3**	0.02
SC_SENS57	ManHorn	0.110	1860.0	30	300	275	**1.5**	0.01
SC_SENS58	ManHorn	0.110	1860.0	30	300	275	**2.0**	0.00
SC_SENS59	ManHorn	0.110	1860.0	30	**75**	150	0.5	0.37
SC_SENS60	ManHorn	0.110	1860.0	30	**225**	150	0.5	0.48
SC_SENS61	ManHorn	0.110	1860.0	30	**375**	150	0.5	0.60
SC_SENS62	ManHorn	0.110	1860.0	30	**450**	150	0.5	0.64
SC_SENS63	ManHorn	0.110	1860.0	30	**525**	150	0.5	0.68
SC_SENS64	ManHorn	0.110	1860.0	30	300	**68**	0.5	0.53
SC_SENS65	ManHorn	0.110	1860.0	30	300	**200**	0.5	0.56
SC_SENS66	ManHorn	0.110	1860.0	30	300	**342**	0.5	0.57
SC_SENS67	ManHorn	0.110	1860.0	30	300	**410**	0.5	0.55
SC_SENS68	ManHorn	0.110	1860.0	30	300	**478**	0.5	0.57
SC_SENS69	ManHorn	**0.027**	1860.0	30	300	275	0.5	0.019
SC_SENS70	ManHorn	**0.082**	1860.0	30	300	275	0.5	0.19
SC_SENS71	ManHorn	**0.138**	1860.0	30	300	275	0.5	0.92
SC_SENS72	ManHorn	**0.165**	1860.0	30	300	275	0.5	0.97
SC_SENS73	ManHorn	**0.193**	1860.0	30	300	275	0.5	0.99
SC_SENS74	ManHorn	0.110	**465**	30	300	275	0.5	0.18
SC_SENS75	ManHorn	0.110	**1395**	30	300	275	0.5	0.45
SC_SENS76	ManHorn	0.110	**2325**	30	300	275	0.5	0.62
SC_SENS77	ManHorn	0.110	**2790**	30	300	275	0.5	0.68
SC_SENS78	ManHorn	0.110	**3255**	30	300	275	0.5	0.73
SC_REG79	Beech	0.180	1198.6	30	350	250	**0.5**	0.96
SC_REG80	Beech	0.180	1198.6	30	350	250	**0.1**	0.97
SC_REG81	Beech	0.180	1198.6	30	350	250	**1.0**	0.17
SC_REG82	Beech	0.180	1198.6	30	**200**	250	0.5	0.94
SC_REG83	Beech	0.180	1198.6	30	**500**	250	0.5	0.98
SC_REG84	Beech	0.180	1198.6	30	350	**10**	0.5	0.90
SC_REG85	Beech	0.180	1198.6	30	350	**450**	0.5	0.99
SC_REG86	Beech	0.180	**424.8**	30	350	250	0.5	0.99

SC_REG87	Beech	0.180	**1972.0**	30	350	250	0.5	0.99
SC_REG88	Beech	**0.110**	1198.6	30	350	250	0.5	0.43
SC_REG89	Beech	**0.250**	1198.6	30	350	250	0.5	0.99
SC_REG90	Beech	0.180	1198.6	**20**	350	250	0.5	1.00
SC_REG91	Beech	0.180	1198.6	**25**	350	250	0.5	0.98
SC_REG92	Beech	0.180	1198.6	**35**	350	250	0.5	0.66
SC_REG93	Beech	0.180	1198.6	**40**	350	250	0.5	0.60
SC_REG94	BroPlant	0.100	395.1	30	350	250	**0.5**	0.09
SC_REG95	BroPlant	0.100	395.1	30	350	250	**0.1**	0.80
SC_REG96	BroPlant	0.100	395.1	30	350	250	**1.0**	0.02
SC_REG97	BroPlant	0.100	395.1	30	**200**	250	0.5	0.10
SC_REG98	BroPlant	0.100	395.1	30	**500**	250	0.5	0.10
SC_REG99	BroPlant	0.100	395.1	30	350	**10**	0.5	0.10
SC_REG100	BroPlant	0.100	395.1	30	350	**450**	0.5	0.08
SC_REG101	BroPlant	0.100	**160.0**	30	350	250	0.5	0.19
SC_REG102	BroPlant	0.100	**972.6**	30	350	250	0.5	0.96
SC_REG103	BroPlant	0.100	395.1	**20**	350	250	0.5	1.00
SC_REG104	BroPlant	0.100	395.1	**25**	350	250	0.5	0.06
SC_REG105	BroPlant	0.100	395.1	**35**	350	250	0.5	0.06
SC_REG106	BroPlant	0.100	395.1	**40**	350	250	0.5	0.06
SC_REG107	EuFir	0.260	1062.0	30	350	250	**0.5**	0.98
SC_REG108	EuFir	0.260	1062.0	30	350	250	**0.1**	0.97
SC_REG109	EuFir	0.260	1062.0	30	350	250	**1.0**	0.23
SC_REG110	EuFir	0.260	1062.0	30	**200**	250	0.5	0.96
SC_REG111	EuFir	0.260	1062.0	30	**500**	250	0.5	0.99
SC_REG112	EuFir	0.260	1062.0	30	350	**10**	0.5	0.98
SC_REG113	EuFir	0.260	1062.0	30	350	**450**	0.5	0.92
SC_REG114	EuFir	0.260	**282.0**	30	350	250	0.5	0.96
SC_REG115	EuFir	0.260	**1842.0**	30	350	250	0.5	1.00
SC_REG116	EuFir	**0.180**	1062.0	30	350	250	0.5	0.86
SC_REG117	EuFir	**0.350**	1062.0	30	350	250	0.5	0.99
SC_REG118	EuFir	0.260	1062.0	**20**	350	250	0.5	1.00
SC_REG119	EuFir	0.260	1062.0	**25**	350	250	0.5	0.99
SC_REG120	EuFir	0.260	1062.0	**35**	350	250	0.5	0.95
SC_REG121	EuFir	0.260	1062.0	**40**	350	250	0.5	0.88
SC_REG122	EuFir	0.260	1062.0	30	300	275	**0.3**	0.94
SC_REG123	EuFir	0.260	1062.0	30	300	275	**0.5**	0.95
SC_REG124	EuFir	0.260	1062.0	30	300	275	**1.0**	0.23
SC_REG125	EuFir	0.260	1062.0	30	**150**	150	0.5	0.88
SC_REG126	EuFir	0.260	1062.0	30	**300**	150	0.5	0.93
SC_REG127	EuFir	0.260	1062.0	30	**600**	150	0.5	0.97
SC_REG128	EuFir	0.260	1062.0	30	300	**137.5**	0.5	0.93
SC_REG129	EuFir	0.260	1062.0	30	300	**550**	0.5	0.93
SC_REG130	EuFir	0.260	**530.0**	30	300	275	0.5	0.84
SC_REG131	EuFir	0.260	**2120.0**	30	300	275	0.5	0.98
SC_REG132	EuFir	**0.130**	1062.0	30	300	275	0.5	0.14

SC_REG133	EuFir	**0.520**	1062.0	30	300	275	0.5	0.99
SC_REG134	EuFir	0.260	1062.0	**20**	300	275	0.5	1.00
SC_REG135	EuFir	0.260	1062.0	**25**	300	275	0.5	0.98
SC_REG136	EuFir	0.260	1062.0	**35**	300	275	0.5	0.87
SC_REG137	EuFir	0.260	1062.0	**40**	300	275	0.5	0.69
SC_REG138	BroPlant	0.100	395.1	30	300	275	**0.3**	0.80
SC_REG139	BroPlant	0.100	395.1	30	300	275	**0.5**	0.09
SC_REG140	BroPlant	0.100	395.1	30	300	275	**1.0**	0.02
SC_REG141	BroPlant	0.100	395.1	30	**150**	150	0.5	0.09
SC_REG142	BroPlant	0.100	395.1	30	**300**	150	0.5	0.09
SC_REG143	BroPlant	0.100	395.1	30	**600**	150	0.5	0.10
SC_REG144	BroPlant	0.100	395.1	30	300	**137.5**	0.5	0.09
SC_REG145	BroPlant	0.100	395.1	30	300	**550**	0.5	0.09
SC_REG146	BroPlant	0.100	**197.5**	30	300	275	0.5	0.05
SC_REG147	BroPlant	0.100	**790.0**	30	300	275	0.5	0.16
SC_REG148	BroPlant	**0.050**	395.0	30	300	275	0.5	0.01
SC_REG149	BroPlant	**0.200**	395.0	30	300	275	0.5	0.65
SC_REG150	BroPlant	0.100	395.0	**20**	300	275	0.5	1.00
SC_REG151	BroPlant	0.100	395.0	**25**	300	275	0.5	0.59
SC_REG152	BroPlant	0.100	395.0	**35**	300	275	0.5	0.19
SC_REG153	BroPlant	0.100	395.0	**40**	300	275	0.5	0.05
SC_REG154	EverBro	0.122	1663.0	42	500	350	0.4	0.84
SC_REG155	ManHorn	0.095	3222.8	37	500	350	0.4	0.81
SC_REG156	EuSpr	0.270	1597.0	40	500	350	0.4	0.98
SC_REG157	ManHorn	0.113	3222.8	43	500	350	0.4	0.62
SC_REG158	ManHorn	0.113	3222.8	41	500	350	0.4	0.64
SC_REG159	LarCemb	0.113	1425.9	39	500	350	0.5	0.89
SC_REG160	EuSpr	0.270	1597.0	35	500	350	0.4	0.99
SC_REG161	EuSpr	0.270	1597.0	38	500	350	0.4	0.99
SC_REG162	Beech	0.178	1972.4	35	500	350	0.4	0.99
SC_REG163	EuSpr	0.270	1597.0	43	500	350	0.4	0.99
SC_REG164	EuSpr	0.270	1597.0	37	500	350	0.4	1.00
SC_REG165	EverBro	0.122	1663.0	43	500	350	0.5	0.55
SC_REG166	EuFir	0.261	1842.0	37	500	350	0.4	1.00
SC_REG167	Ripar	0.187	308.0	43	500	350	0.5	0.85
SC_REG168	Beech	0.178	1972.4	45	500	350	0.4	0.98
SC_REG169	EuSpr	0.270	1597.0	42	500	350	0.4	0.99
SC_REG170	Chest	0.198	1879.7	34	500	350	0.4	0.99
SC_REG171	Beech	0.178	1972.4	33	500	350	0.5	0.99
SC_REG172	Ripar	0.187	1540.8	45	500	350	0.4	0.99
SC_REG173	LarCemb	0.222	1425.9	34	500	350	0.5	1.00
SC_REG174	LarCemb	0.222	1425.9	38	500	350	0.4	1.00
SC_REG175	Ripar	0.187	1540.8	40	500	350	0.4	0.99
SC_REG176	LarCemb	0.222	1425.9	39	500	350	0.4	1.00
SC_REG177	EuSpr	0.270	1597.0	37	500	350	0.4	1.00
SC_REG178	LarCemb	0.222	1425.9	23	200	350	0.5	0.97

SC_REG179	LarCemb	0.222	1425.9	30	200	350	0.4	0.99
SC_REG180	Scots	0.168	40.4	40	500	350	0.5	0.01